DAC-62279

A TIME-DEPENDENT APPROACH TO THE NUMERICAL SOLUTION OF THE FLOW FIELD ABOUT AN AXISYMMETRIC VEHICLE AT ANGLE OF ATTACK

FINAL REPORT

June 1968

Prepared under Contract No. NAS 8-21141
by Douglas Aircraft Company
Missile and Space Systems Division
Santa Monica, California
for
GEORGE C. MARSHALL SPACE FLIGHT CENTER
HUNTSVILLE, ALABAMA 35812

DAC-62279

A TIME-DEPENDENT APPROACH TO THE NUMERICAL SOLUTION OF THE FLOW FIELD ABOUT AN AXISYMMETRIC VEHICLE AT ANGLE OF ATTACK

FINAL REPORT

June 1968

By
J. XERIKOS
W. A. ANDERSON

Prepared under Contract No. NAS 8-21141
by Douglas Aircraft Company
Missile and Space Systems Division
Santa Monica, California
for
GEORGE C. MARSHALL SPACE FLIGHT CENTER
HUNTSVILLE, ALABAMA 35812

This report was prepared by Douglas Aircraft Company under Numerical Solution of Special Flow Problems for Saturn Vehicles, Contract No. NAS8-21141, for the George C. Marshall Space Flight Center of the National Aeronautics and Space Administration. The work was administered under the technical direction of the Aero-Astrodynamics Laboratory.

ABSTRACT

A three-dimensional inviscid flow field analysis for treating axisymmetric configurations at angle of attack has been formulated and mechanized in the form of a Fortran IV UNIVAC 1108 computer program. A time-dependent floating mesh technique is employed which involves use of a conditionally stable, first-order finite difference representation of the governing equations. Provisions are included for treating an axisymmetric flare located on the vehicle afterbody. Computations have been performed for sphere and sphere-cone configurations as well as for a hemi-cylindrical flare in a uniform free stream. A significant feature of the results is that the three-dimensional mode of calculation does not appear to introduce unstable behavior in cases which can be run successfully at zero angle of attack. The applicable range and accuracy of the computer program are discussed with respect to free stream and vehicle geometry parameters.

CONTENTS

LIST OF FIGURES

SYMBOLS

a	Speed of sound
A	Matrix with elements $A_{ij} = \partial F_i / \partial \upsilon_j$
B	Body surface, $x = B(r)$
C	Coordinate system base surface, $x = C(r)$
C_s, C_n, C_ϕ	Damping term coefficients
$\overline{C}$	Time step factor
D	Geometric factor, $\Delta s_{\ell+1} / \Delta s_\ell$
e	Specific internal energy
$\vec{e}_\alpha$, $\vec{e}_\beta$, $\vec{e}_\gamma$	Unit vectors in α, β, γ directions, respectively
E	Nondimensional specific total energy, $\frac{\overline{E}}{V_\infty{}^2}$
f	Distance between surfaces B and C measured in n-direction
F	Distance between surfaces W and C measured in n-direction
g	Shock surface, $g(s, n, \phi, t) = 0$
h	Nondimensional specific enthalpy, $\bar{h} / V_\infty{}^2$
h_α, h_β, h_γ	Transformation scale factors
G, H	Functions defined in Equation 2-3
κ	Integer index, $s = (\kappa - 1)\Delta s$
K	Damping term factor
M_∞	Free-stream Mach number
M, N, P, Q	Vector functions of U defined in Equation 2-1
$\vec{N}$	Shock surface unit normal vector
p	Nondimensional pressure, $\frac{\bar{p}}{\rho_\infty V_\infty{}^2}$
q	Arbitrary flow property (Appendix D)
R_N	Vehicle nose radius
R	Coordinate system base surface radius of curvature

t	Nondimensional time, $\bar{t}V_\infty/R_N$
U	Conservation variable defined in Equation 2-1
U_s	Shock velocity
u	Velocity component normal to shock wave (Appendix B)
v_α, v_β, v_γ	Nondimensional velocity components in α, β, γ directions, respectively
V	Nondimensional total velocity, $\frac{\bar{V}}{V_\infty}$
V_N	Nondimensional velocity component normal to shock surface
V_T	Nondimensional velocity component tangent to shock surface
W	Shock surface, $n = W(s, \phi, t)$
α	Angle of attack
$\beta_s, \beta_n, \beta_\phi$	Angles measured between $\vec{N}$ and s, n, and ϕ coordinate axes, respectively
γ	Ratio of specific heats, c_p/c_v
ϵ_o	Shock detachment distance at axis of body
θ	Coordinate system reference surface angle measured from body axis
θ_B	Body surface angle measured from body axis
μ	Artificial viscosity coefficient
ρ	Nondimensional density, $\frac{\bar{\rho}}{\rho_\infty}$
χ	Spatial coordinate given in Equation 3-1
υ	Conservation variable defined in Equation 3-1

Coordinate Systems

$\{x, r, \phi\}$	Cylindrical polar coordinates
$\{\alpha, \beta, \gamma\}$	Generalized curvilinear orthogonal coordinates
$\{s, n, \phi\}$	Cylindrical curvilinear coordinates
$\{\tilde{s}, \tilde{n}, \tilde{\phi}\}$	Shock layer transformation coordinates

Superscript

κ	Time index

Subscripts

ℓ, m, n	Spatial indices for s, n, ϕ directions, respectively
α, β, γ	Values in α, β, γ directions, respectively
B	Body surface value
∞	Free-stream condition
o	Condition ahead of shock (Appendix B)
t	Stagnation value
N	Conditions behind normal shock
F	Flare value

Section 1
INTRODUCTION

During the past several years, a new class of time-dependent computational techniques has been developed and applied to the solution of steady-state fluid flow problems. These methods are largely based on physical and mathematical concepts originally derived in treating unsteady flow phenomena. Continuing improvements in computer technology have increased the economic feasibility of performing the large-scale calculations associated with these methods. A brief review of developments that lead to the present computational state of the art is given below.

Because of the difficulty involved in numerically solving the unsteady equations of fluid motion in the presence of moving boundaries (shock waves) across which flow properties are discontinuous, a technique was developed by J. von Neumann in 1949 (Reference 1) wherein artificial dissipative terms were explicitly introduced which had the effect of "smearing out" the discontinuities. This eliminated the necessity for locating these surfaces in space and time during the calculation to apply special boundary conditions along them.

Following further mathematical development in the area of dissipative finite difference schemes (See Reference 2 for a comprehensive discussion of this topic), many fluid flow problems were successfully attacked using this approach. In practice, the method involves a fixed network of mesh points within which discrete discontinuities such as shock waves appear as moving disturbances covering several mesh points in width. In particular, computations were performed at the Rand Corporation (Reference 3) and at the Los Alamos Scientific Laboratory (LASL). Topics treated by the latter include various two-dimensional problems involving solutions of the Navier-Stokes equations, for example, Reference 4. The continuing work at LASL

involves unique Eulerian (fixed mesh or cells) and Lagrangian (particle tracing) approaches. Recently, Bohachevsky (Reference 5) has used a fixed mesh method to compute the flow field about axisymmetric bodies at angle of attack. The results of this study emphasized the somewhat prohibitive computing time requirements associated with highly damped, fixed mesh, time-dependent techniques.

In 1959, Godunov (Reference 6) introduced the floating mesh concept for the treatment of blunt bodies in a supersonic stream in which the shock is treated as a true discontinuity and the finite difference mesh is uniformly distributed between the shock and the body. He used a sophisticated differencing technique involving linearized simple wave relations and obtained a steady-state flow field in asymptotic fashion. During the "starting process", artificial viscosity relations within the shock layer were used to damp out the transient waves arising from the suddenly imposed supersonic free stream. Subsequently, Babenko et al., (Reference 7) used a floating mesh approach to compute the steady-state flow field about pointed cones at angle of attack. Moretti (Reference 8) has employed a similar technique to treat blunted cones and ellipsoids at angle of attack using characteristic relations at the shock and body in connection with a second-order finite difference scheme similar to that developed by Lax and Wendroff (Reference 9). Masson (Reference 10) has recently applied the Godunov method to the computation of flow fields about planar and axisymmetric blunt bodies in supersonic flow.

All of the preceding methods have, at least in part, attempted to describe the asymptotic process in time so that a natural transition to steady state occurs during the calculation. Crocco (Reference 11) has examined the time-dependent approach and has emphasized the inherent computational advantages; for example, the governing unsteady differential equations are hyperbolic in the subsonic and sonic regimes as well as in the supersonic regime. Thus, mixed flow two-point boundary value problems involving singularities (e.g., blunt-body direct integral method) may be formulated as singularity-free initial value problems. Further, considering time as a purely iterative variable, the asymptotic approach to steady state may not be related to an unsteady flow process found in nature.

The present study is concerned with the application of time-dependent finite difference techniques to the solution of the steady-state, inviscid flow field about an axisymmetric vehicle at angle of attack in a supersonic free stream. Provisions have been included for treating a body flare with detached shock wave (transonic flare). A floating mesh approach has been used to describe accurately bow and flare shock waves as discrete surfaces across which flow property discontinuities are specified by exact moving shock relations. The principal objective of the study is to develop an operational computer program capable of generating an accurate three-dimensional flow field description given initial data consisting of vehicle geometry, free-stream conditions, and angle of attack. Although the analytical formulation and the selection of the finite difference analog of the governing equations are guided by the results of linear stability theory, a significant degree of numerical experimentation is involved because the present multidimensional problem is highly nonlinear.

Section 2

ANALYTICAL DEVELOPMENT OF GOVERNING EQUATIONS

2.1 GOVERNING EQUATIONS IN CYLINDRICAL CURVILINEAR COORDINATES

The equations describing the unsteady, inviscid, adiabatic flow of gas in cylindrical curvilinear coordinates can be represented in the conservation-law form (see Appendix A):

$$\frac{\partial \bar{U}}{\partial t} + \frac{\partial \bar{M}}{\partial s} + \frac{\partial \bar{N}}{\partial n} + \frac{\partial \bar{P}}{\partial \phi} + Q = 0 \qquad (2\text{-}1)$$

where

$$\bar{U} = r\left(1 + \frac{n}{R}\right)\begin{bmatrix} \rho \\ \rho v_s \\ \rho v_n \\ \rho v_\phi \\ \rho E \end{bmatrix} = r\left(1 + \frac{n}{R}\right)U \quad , \quad \bar{M} = r\begin{bmatrix} \rho v_s \\ \rho v_s^2 + p \\ \rho v_s v_n \\ \rho v_s v_\phi \\ \rho v_s (E + p/\rho) \end{bmatrix} = rM \quad ,$$

$$\bar{N} = r\left(1+\frac{n}{R}\right)\begin{bmatrix} \rho v_n \\ \rho v_n v_s \\ \rho v_n^2 + p \\ \rho v_n v_\phi \\ \rho v_n (E + p/\rho) \end{bmatrix} = r\left(1+\frac{n}{R}\right)N \quad , \quad \bar{P} = \left(1+\frac{n}{R}\right)\begin{bmatrix} \rho v_\phi \\ \rho v_\phi v_s \\ \rho v_\phi v_n \\ \rho v_\phi^2 + p \\ \rho v_\phi (E + p/\rho) \end{bmatrix} = \left(1+\frac{n}{R}\right)P \quad ,$$

$$Q = \begin{bmatrix} 0 \\ \dfrac{r\rho v_s v_n}{R} - \left(1 + \dfrac{n}{R}\right)\sin\theta\,(\rho v_\phi^2 + p) \\ -\left(1 + \dfrac{n}{R}\right)\cos\theta\,(\rho v_\phi^2 + p) - \dfrac{r}{R}(\rho v_s^2 + p) \\ \left(1 + \dfrac{n}{R}\right)\rho v_\phi\,(v_s \sin\theta + v_n \cos\theta) \\ 0 \end{bmatrix}$$

and, for a perfect gas,

$$p = (\gamma-1)\left|\rho E - \frac{1}{2\rho}\left[(\rho v_s)^2 + (\rho v_n)^2 + (\rho v_\phi)^2\right]\right|. \qquad (2-2)$$

Since $p = p(U)$, the vector functions M, N, P, and Q can be expressed entirely as functions of the conservation variables U.

2.2 TRANSFORMATION TO SHOCK LAYER COORDINATES

A basic consideration involved in the choice of a coordinate system is that a finite difference network can be conveniently described which is uniformly distributed between the shock and body. To establish a shock layer coordinate system which is not excessively distorted by the presence of an extremely blunt nose or a sharp corner, an arbitrary reference surface C(r) is established which intersects the axis of symmetry normally and serves as the base for the curvilinear coordinate system (s, n, ϕ)(Figure 2-1). For a smooth (continuous slope) blunt body, B(r) and C(r) can be required to coincide for convenience. The finite difference network is distributed between the shock wave W(s, ϕ, t) and the body with Δn = constant at a given value of s, i.e., the shock layer is subdivided into an arbitrary number of equally spaced strips.

A shock layer transformation, based on the preceding considerations, can be defined by the relations (see Figure 2-2)

$$\tilde{s} = s$$

$$\tilde{n} = \frac{n - f(s)}{F(s, \phi, t) - f(s)} = \frac{j}{S}$$

$$\tilde{\phi} = \phi$$

$$\tilde{t} = t$$

where $j = 0, 1, 2, \ldots, S$ with S = number of shock layer strips. It follows that the body and shock wave are given by $\tilde{n} = 0$ and $\tilde{n} = 1$, respectively, in the transformed system. Performing the transformation, the governing Equations 2-1 take the form

$$\frac{\partial \overline{U}}{\partial \tilde{t}} + \frac{\partial \overline{M}}{\partial \tilde{s}} + \frac{\partial \overline{P}}{\partial \tilde{\phi}} + G\frac{\partial F}{\partial t}\frac{\partial \overline{U}}{\partial \tilde{n}} + H\frac{\partial \overline{M}}{\partial \tilde{n}} + \frac{1}{F-f}\frac{\partial \overline{N}}{\partial \tilde{n}} + G\frac{\partial F}{\partial \phi}\frac{\partial \overline{P}}{\partial \tilde{n}} + Q = 0 \qquad (2-3)$$

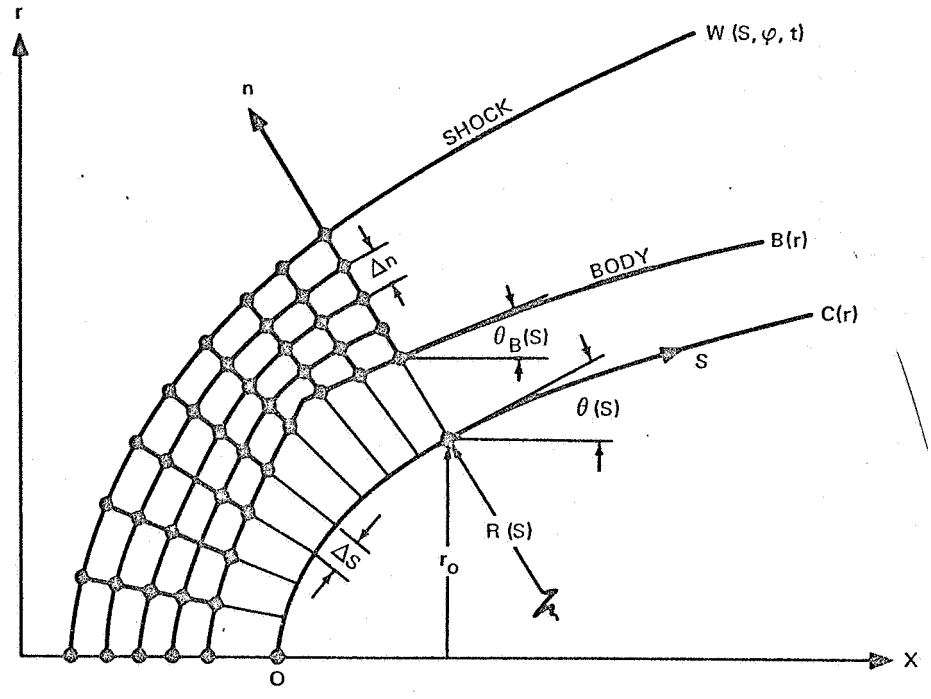

Figure 2-1. Coordinate System Description

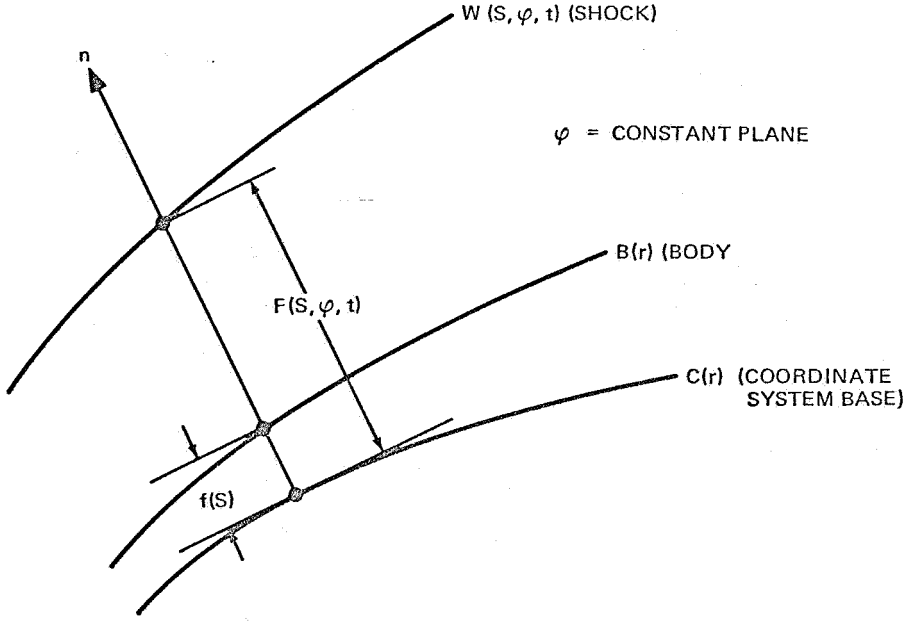

Figure 2-2. Shock Layer Geometric Parameters

where

$$G(s, n, \phi, t) = -\frac{n-f}{(F-f)^2}$$

$$H(s, n, \phi, t) = -\frac{1}{F-f}\frac{\partial f}{\partial s} + G\left(\frac{\partial F}{\partial s} - \frac{\partial f}{\partial s}\right)$$

The specification of explicit analytical expressions for the body and coordinate system base surfaces enables determination of f(s). Subsequently, df/ds is obtained from

$$\frac{df}{ds} = \left(1 + \frac{f}{R}\right) \tan\left(\theta_B - \theta\right) \qquad (2\text{-}4)$$

The temporal derivative $\partial F/\partial t$ can be expressed in terms of the shock velocity and the spatial derivatives $\partial F/\partial s$ and $\partial F/\partial \phi$ (see Subsection 2.3). Evaluation of $\partial F/\partial s$ and $\partial F/\partial \phi$ requires the introduction of a finite difference approximation for these partial derivatives in the ϕ = constant and s = constant planes, respectively.

2.3 SPECIFICATION OF BOUNDARY CONDITIONS

2.3.1 Shock Surface

The Rankine-Hugoniot relations for a moving three-dimensional shock surface (derived in Appendix B) are applied at the bow and flare shock waves. The shock velocity $U_s(s, \phi, t)$ serves as a control function during the asymptotic convergence process. U_s is measured in the direction of the normal $\vec{N}$ to the shock surface at time t.

Referring to Figure 2-3,

$$\frac{\partial}{\partial t}(F-f) = \frac{\partial F}{\partial t} = U_s \cos\beta_n$$

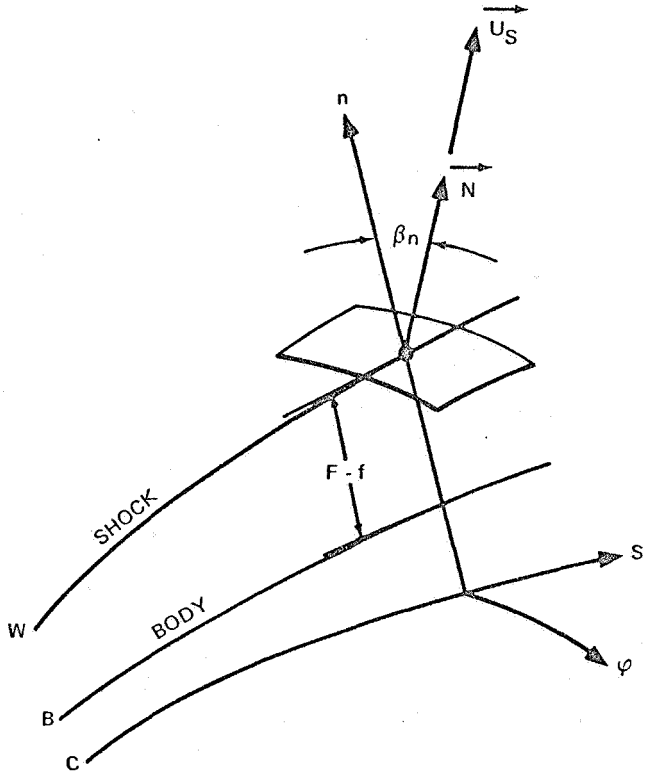

Figure 2-3. Shock Velocity Orientation

Defining the shock surface by $g(s, n, \phi, t) = 0$,

$$\cos\beta_n = \frac{1}{G}\frac{\partial g}{\partial n} , \quad G = |\nabla g|$$

Let $g = n - F(s, \phi, t) = 0$.

Then

$$\frac{\partial F}{\partial t} = \frac{U_s}{G} , \quad G = \left[\frac{1}{\left(1+\frac{F}{R}\right)^2} \left(\frac{\partial F}{\partial s}\right)^2 + 1 + \frac{1}{r_s^2}\left(\frac{\partial F}{\partial \phi}\right)^2 \right]^{1/2}$$

where (2-5)

$$r_s = r_o + F\cos\theta$$

2.3.2 Body Surface

The only rigorous condition which can be specified on the body surface during the time-dependent flow process is that the normal component of velocity

vanishes. This condition provides a relationship between the velocity components v_s and v_n at the body (v_{ϕ_B} is tangent to the body):

$$v_{n_B} = v_{s_B} \tan(\theta_B - \theta) \tag{2-6}$$

2.3.3 Convex Corner

Independent of the coordinate system used, the influence of a discontinuity in body slope (convex corner) can only be approximately described with a finite difference mesh unless auxiliary analytical relations are provided at the corner. In the axisymmetric case, for example, it is possible to relate upstream and downstream flow properties and their rates of change along the body surface using exact inviscid equations (Reference 12). In a more general approach, a description of flow properties both on and off the body near a convex corner based on the analysis of Reference 13 has been adapted (Reference 14) for use with an integral method solution of extremely blunt-nosed, e.g., flat-faced, axisymmetric body flow fields. For the three-dimensional case, comparable analyses would be required which, if developed, could introduce prohibitive complexity in asymmetric flow calculations. In the present approach, therefore, the corner description primarily involves enforcement of upstream and downstream body surface boundary conditions.

2.3.4 Axis of Symmetry

Calculations at the body axis, which is common to all meridianal planes, require special treatment because of the singular behavior of certain terms in the governing equations as $r \to 0$. This behavior is purely a function of the choice of coordinate system and persists for both symmetric ($\alpha = 0$) and asymmetric ($\alpha > 0$) flow cases. A special form of these equations which is valid at the axis of symmetry has been derived and is presented in Appendix C. For the asymmetric flow case, the axis (given by $r = 0$) is a regular line in the flow field with no applicable symmetry conditions other than those associated with the $\phi = 0$ and $\phi = \Pi$ planes. The finite difference relations at mesh points contained in the flow field plane of symmetry reflect

appropriate symmetric or antisymmetric functional behavior for each flow property.

2.4 BODY FLARE ANALYSIS

A convenient geometrical scheme for describing the shock layer is to transform it into a cylindrical region as in the present analysis. The presence of an axisymmetric body frustum or flare complicates the shock layer geometry by introducing a second region bounded by the flare shock, the body, and an arbitrary downstream station. In addition, a weak secondary shock or expansion wave may appear at intersection of the bow and flare shocks which equalize the pressure and flow direction on either side of the slip line emanating from the intersection.

A tractable approach to the two region problem involves a sequential convergence procedure. Initially a single shock, floating mesh solution for the nose and afterbody region can be obtained neglecting the presence of the flare. A test of the flow conditions at the location corresponding to the base of the flare establishes whether the flare shock is attached or detached (transonic flare). A flare and afterbody solution can then be carried out to the next flare location or to the base of the vehicle using the computer stored non-uniform conditions ahead of the flare shock (see Appendix D). This approach has the following advantages: (1) for a given nose-afterbody solution, a parametric series of frustrum calculations can be performed consecutively, changing, for example, the frustum angle or location; (2) after a time-dependent floating flare shock subroutine is developed, bodies with several flares can be treated.

The procedure described above has been employed in the present study. The flare solution is obtained using the previously developed governing equations and a new coordinate system base surface $C_F(r)$ which intersects the afterbody normally (Figure 2-4). The special form of the governing equations is not required in the flare calculation as $r>o$.

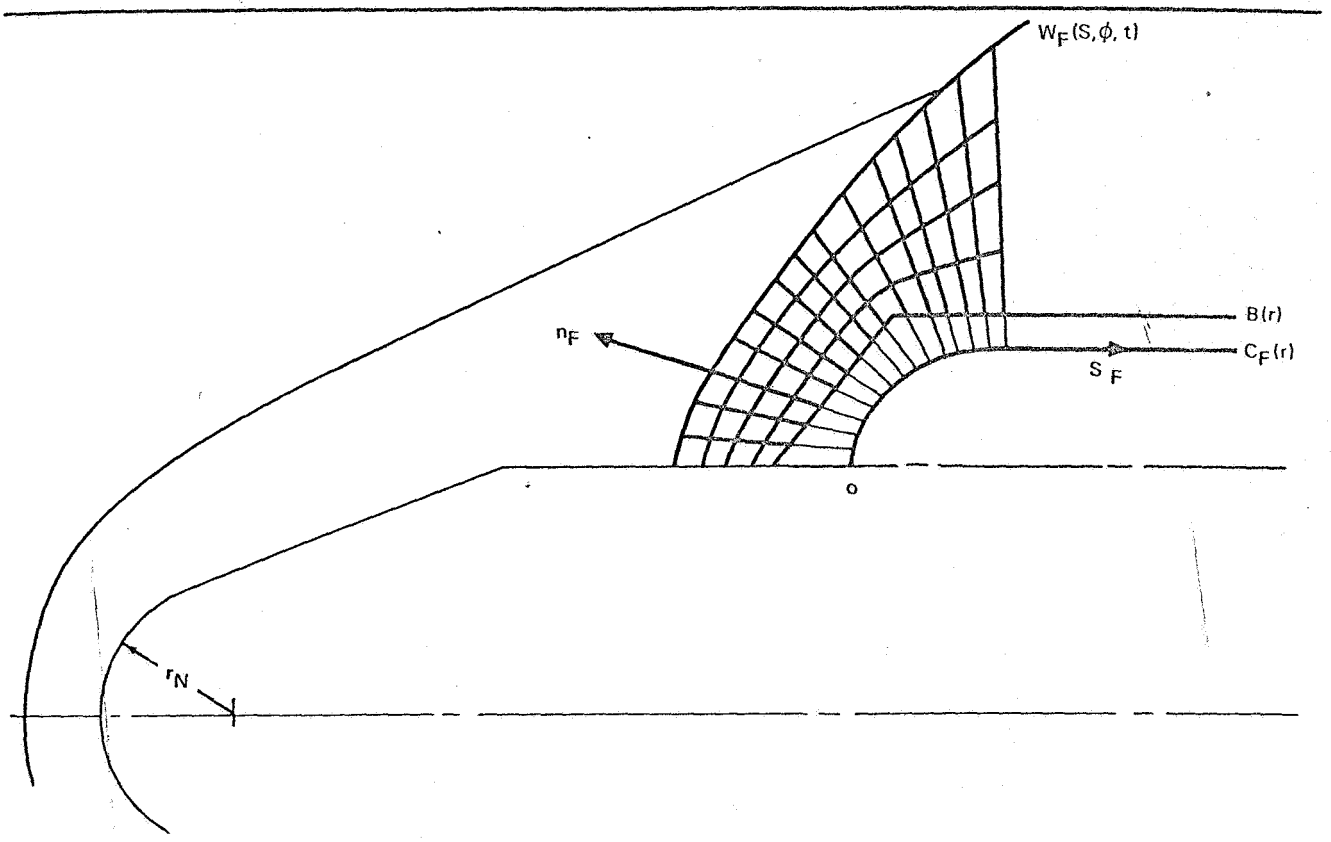

Figure 2-4. Flare Coordinate System

Section 3

FINITE DIFFERENCE REPRESENTATION OF GOVERNING EQUATIONS

3.1 GENERAL CONSIDERATIONS

The various numerical schemes for representation of time and space derivatives in finite difference form can be broadly categorized (for a given class of differential equations) as being either unconditionally or conditionally stable in terms of a given time step Δt. Unconditionally stable methods are implicit in that each time step requires an iteration involving values of the dependent variables at both times t_o and $t_1 > t_o$, for example, $t_1 = t_o + \Delta t$. Because there are no stability limitations on the magnitude of Δt, accuracy requirements and the time rate of change of boundary conditions establish a practical limit on the size of the time step. Implicit methods are usually applied to unsteady flow problems that require an accurate stepwise description of a time-dependent process.

Conditionally stable methods are subject to the requirement that the magnitude of a given time step does not exceed a value expressed in terms of the mesh geometry and the dependent variables involved in the problem. For example, $\Delta t \leqq \Delta X/(|u| + a)$ is the well-known von Neumann stability condition for a linear one-dimensional fluid flow problem where u = velocity and a = sound speed.

The finite difference methods applied to the present study are in the conditionally stable category. As the governing partial differential equations are nonlinear, it is not possible to establish exact stability requirements on Δt. In addition the multidimensional aspects of the problem preclude direct use of existing mathematical results which are typically based upon one- or two-dimensional analyses involving uniformly spaced, orthogonal finite difference networks. In spite of the idealizations employed, stability requirements based upon linear theory can serve as a useful guide in specifying stable time step magnitudes during the computations.

A brief description of several conditionally stable finite difference schemes of first- and second-order accuracy is presented below as applied, for simplicity, to the one-dimensional vector equation.

$$\frac{\partial \upsilon}{\partial t} + \frac{\partial F}{\partial X}(\upsilon) = 0 \tag{3-1}$$

(See, for example, Reference 2 for a detailed treatment of these methods.)

3.2 LAX-WENDROFF SECOND-ORDER SCHEME

The Lax-Wendroff finite difference equations are basically derived from a truncated Taylor's series in t, i. e.,

$$\upsilon_\ell^{\kappa+1} = \upsilon_\ell^\kappa + \left(\frac{\partial \upsilon}{\partial t}\right)_\ell^\kappa \Delta t + \left(\frac{\partial^2 \upsilon}{\partial t^2}\right)_\ell^\kappa \frac{(\Delta t)^2}{2} \tag{3-2}$$

where the superscripts represent a time index and the subscripts a spatial index, e. g.,

$$\upsilon_{\ell+1}^{\kappa+1} = \upsilon(X_\ell + \Delta X,\ t_\kappa + \Delta t)$$

In general, the time derivatives are replaced by spatial derivatives through use of the governing equations and associated boundary conditions. Defining the matrix $A(\upsilon)$ as the Jacobian of F with respect to υ with elements $A_{ij} = \partial F_i / \partial \upsilon_j$, Equation 3-2 becomes

$$\upsilon_\ell^{\kappa+1} = \upsilon_\kappa^\ell - \left(\frac{\partial F}{\partial X}\right)_\ell^\kappa \Delta t + \frac{\partial}{\partial X}\left(A \frac{\partial F}{\partial X}\right)_\ell^\kappa \frac{(\Delta t)^2}{2} \tag{3-3}$$

Considering A to be a constant matrix, use of conventional difference quotients for the X-derivatives in Equation 3-3 yields

$$\upsilon_\ell^{\kappa+1} = \upsilon_\ell^\kappa - \frac{1}{2} A \frac{\Delta t}{\Delta X}\left(\upsilon_{\ell+1}^\kappa - \upsilon_{\ell-1}^\kappa\right) + \frac{1}{2}\left(A \frac{\Delta t}{\Delta X}\right)^2 \left(\upsilon_{\ell+1}^\kappa - 2\upsilon_\ell^\kappa + \upsilon_{\ell-1}^\kappa\right) \tag{3-4}$$

The conditional stability of the system of finite difference Equation 3-4 has been established. Specifically, the von Neumann condition has been found to be both necessary and sufficient for stability.

3.3 TWO-STEP LAX-WENDROFF SCHEME

The two-step Lax-Wendroff procedure offers the advantage of second-order accuracy through the application of two first-order calculations for each time step. In particular, the matrix A need not be evaluated during the calculation.

For each point in the mesh, one initially obtains intermediate data at $(X_\ell + \frac{1}{2}\Delta X,\ t_\kappa + \frac{1}{2}\Delta t)$ using the relation

$$\upsilon_{\ell+\frac{1}{2}}^{\kappa+\frac{1}{2}} = \frac{1}{2}\left(\upsilon_{\ell+1}^{\kappa} + \upsilon_{\ell}^{\kappa}\right) - \frac{\Delta t}{2\Delta X}\left(F_{\ell+1}^{\kappa} - F_{\ell}^{\kappa}\right) \tag{3-5}$$

Final values at $(X_\ell,\ t_\kappa + \Delta t)$ are then calculated using

$$\upsilon_{\ell}^{\kappa+1} = \upsilon_{\ell}^{\kappa} - \frac{\Delta t}{\Delta X}\left(F_{\ell+\frac{1}{2}}^{\kappa+\frac{1}{2}} - F_{\ell-\frac{1}{2}}^{\kappa+\frac{1}{2}}\right) \tag{3-6}$$

For the special case $F(\upsilon) = A\upsilon$, substitution of Equation 3-5 into Equation 3-6 yields the second-order Lax-Wendroff relation Equation 3-4. It should be noted that variations on the two-step Lax-Wendroff scheme have been developed (see, for example, Reference 15).

3.4 LAX FIRST-ORDER SCHEME

A conditionally stable first order difference scheme introduced by Lax (Reference 16) expresses Equation 3-1 in the form

$$\upsilon_{\ell}^{\kappa+1} = \frac{1}{2}\left[\upsilon_{\ell+1}^{\kappa} + \upsilon_{\ell-1}^{\kappa}\right] - \frac{\Delta t}{2\Delta X}\left(F_{\ell+1}^{\kappa} - F_{\ell-1}^{\kappa}\right) \tag{3-7}$$

Note that Equation 3-7 is almost identical to the intermediate relation used in the two-step Lax-Wendroff method. The forward time difference in Equation 3-7 can be rewritten as

$$\left(\frac{\partial \upsilon}{\partial t}\right)_{\ell}^{\kappa} = \frac{\upsilon_{\ell}^{\kappa+1} - \upsilon_{\ell}^{\kappa}}{\Delta t} - \frac{(\Delta X)^2}{2\Delta t}\left[\frac{\upsilon_{\ell-1}^{\kappa} + \upsilon_{\ell+1}^{\kappa} - 2\upsilon_{\ell}^{\kappa}}{(\Delta X)^2}\right] \tag{3-8}$$

As the second term can be interpreted as the conventional finite difference representation of a second derivative with respect to X, the coefficient of this term, by analogy with a second-order viscous term, is often referred to

as an "artificial viscosity" coefficient, $\mu = (\Delta X)^2/2\Delta t$. In two dimensions, the "dissipative" term takes the form of a Laplacian in rectangular coordinates. Terms appearing in this form will be referred to as damping terms in the remainder of the report.

Following Reference 5, a three-dimensional version of the first-order Lax scheme has been used in the present study. The finite difference time and space derivative operators are given below.

$$\left[\frac{\partial \upsilon s}{\partial t}\right]^K_{\ell, m, n} = \frac{1}{\Delta t}\left\{\upsilon^{K+1}_{\ell, m, n} - \upsilon s^K_{\ell, m, n} - K\left[\left(\upsilon s^K_{\ell+1, m, n} + \upsilon^K_{\ell-1, m, n} - 2\upsilon s^K_{\ell, m, n}\right) C_s + \left(\upsilon s^K_{\ell, m+1, n} + \upsilon s^K_{\ell, m-1, n} - 2\upsilon s^K_{\ell, m, n}\right) C_n + \left(\upsilon s^K_{\ell, m, n+1}, + \upsilon s^K_{\ell, m, n-1} - 2\upsilon s^K_{\ell, m, n}\right) C_\phi\right]\right\} \quad (3\text{-}9)$$

where

$$\upsilon^{K+1}_{\ell+1, m+1, n+1} = \upsilon(s_\ell + \Delta s,\ n_m + \Delta n,\ \phi_n + \Delta\phi,\ t^K + \Delta t)$$

$K = \frac{1}{4}$, $C_\phi = 0$ for axisymmetric case

$K = \frac{1}{6}$ for $\alpha > 0$

The damping term factors C_s, C_n, and C_ϕ are equal either to unity or zero. For a general field point $C_s = C_n = C_\phi = 1$. At the network boundaries (shock, body, axis of symmetry, and downstream exit plane), the C's are set in accordance with appropriate boundary conditions. No geometric factors involving mesh dimensions are introduced in the time derivative. It has been pointed out (Reference 5) that in an axisymmetric case, use of geometric scale factors corresponding to those appearing in the definition of a Laplacian in cylindrical coordinates did not alter the final results of the time-dependent, fixed-mesh calculations.

The spatial derivatives are given in terms of the central difference operators:

$$\left(\frac{\partial F}{\partial s}\right)^{K}_{\ell, m, n} = \frac{1}{2\Delta s}\left[F^{K}_{\ell+1, m, n} - F^{K}_{\ell-1, m, n} \right], \quad \Delta s = \text{constant}$$

$$\left(\frac{\partial F}{\partial n}\right)^{K}_{\ell, m, n} = \frac{1}{2\Delta n}\left[F^{K}_{\ell, m+1, n} - F^{K}_{\ell, m-1, n}\right]$$

$$\left(\frac{\partial F}{\partial \phi}\right)^{K}_{\ell, m, n} = \frac{1}{2\Delta \phi}\left[F^{K}_{\ell, m, n+1} - F^{K}_{\ell, m, n-1}\right]$$

If Δs is specified as a geometrically increasing function of s, a weighted average finite difference relation is used for evaluating $\partial F/\partial s$, e. g. ,

$$\Delta s_{\ell} = s_{\ell} - s_{\ell-1} = \Delta s_{o}(D)^{\ell-1}, \quad D = (\Delta s_{\ell+1} / \Delta s_{\ell}), \quad \Delta s_{o} = \text{constant}$$

$$\left(\frac{\partial F}{\partial s}\right)^{K}_{\ell, m, n} = \frac{\frac{1}{D^2}\left(F^{K}_{\ell+1, m, n} - F^{K}_{\ell, m, n}\right) + F^{K}_{\ell, m, n} - F^{K}_{\ell-1, m, n}}{\Delta s_{\ell}\left(1 + \frac{1}{D}\right)}$$

At the boundaries, for a given space variable χ_i, one-sided difference operators are used if the function is odd in χ_i (i. e. , $F(\chi_i) = -F(-\chi_i)$) while a zero value is assigned for the χ_i - derivative if the function is even in χ_i ($F(\chi_i) = F(-\chi_i)$). For example, in the flow field plane of symmetry, v_s, v_n, p , ρ , and E are even functions in ϕ while v_ϕ is an odd function in ϕ.

Section 4
COMPUTER PROGRAM DESCRIPTION

The basic features of the Fortran IV, UNIVAC 1108 computer program which provides a numerical solution of the governing finite difference equations are briefly described in this section.

4.1 PROGRAM INPUTS

The inputs required to perform the forebody calculation include:

1. Free-stream Mach number, M_∞
2. Ratio of specific heats, γ
3. Angle of attack, α
4. Initial shock detachment distance at axis, ϵ_o
5. s-direction mesh interval factors, Δs_o, D
6. Number of s-planes ($\leqq 40$)
7. Number of n-planes ($\leqq 5$)
8. Number of ϕ-planes ($\leqq 9$)

The body geometry can be input by specifying either (1) x_o, r_o, θ, R, f, x_B, r_B, θ_B as arbitrary functions of s or (2) s_{cone}, θ_c, and $s_{cylinder}$ which define a sphere-cone-cylinder (Figure 4-1a). For a flare calculation, the additional geometric information required is the preflare body angle and the coordinates (x_F, r_F) (Figure 4-1b). The number of s and n planes used in the flare network can differ from those employed in the upstream forebody calculation; however, the number of ϕ-planes must remain constant.

A number of input flags are available which offer the option, following the completion of a forebody calculation, of (1) stopping, (2) calling in a new case, or (3) initiating a flare calculation using nonuniform upstream shock layer conditions. In addition, a flare calculation can be performed directly using uniform free-stream conditions. Other input flags allow use of previously calculated flow field properties as initial values for a new case.

$$S_{CONE} = \sum_{\ell=1}^{\eta} \Delta S_\ell$$

$$S_{CYLINDER} = \sum_{\ell=1}^{\zeta} \Delta S_\ell - 1/2\,\Delta S_\zeta$$

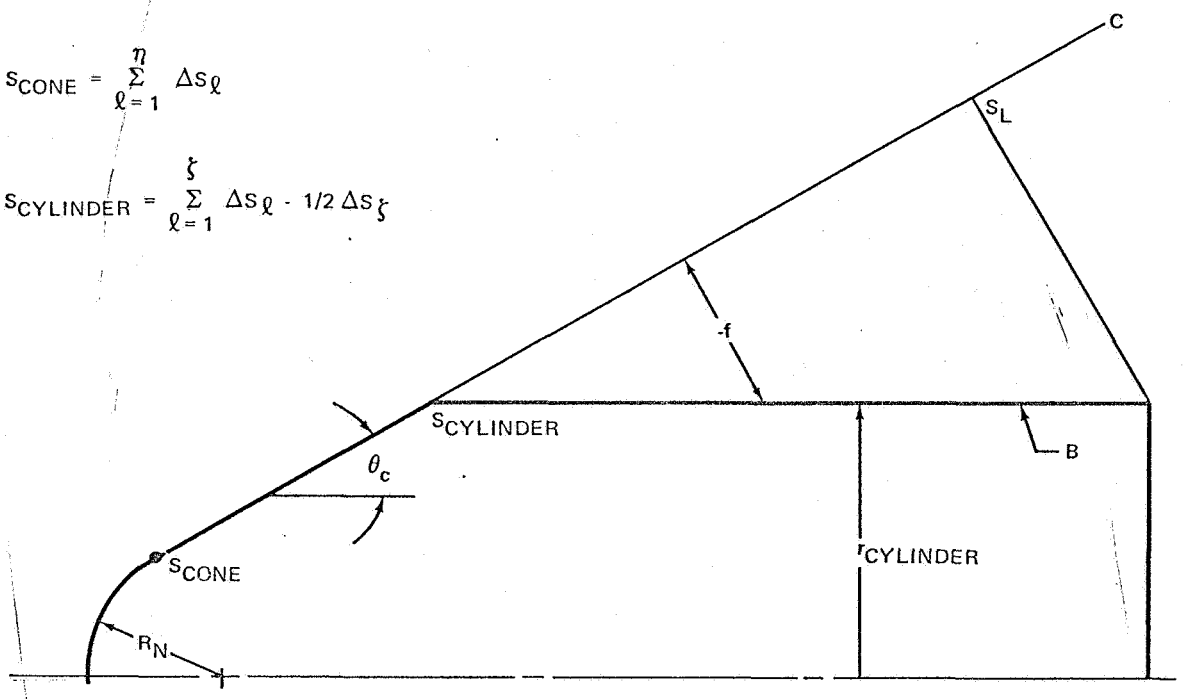

(a) FOREBODY GEOMETRY

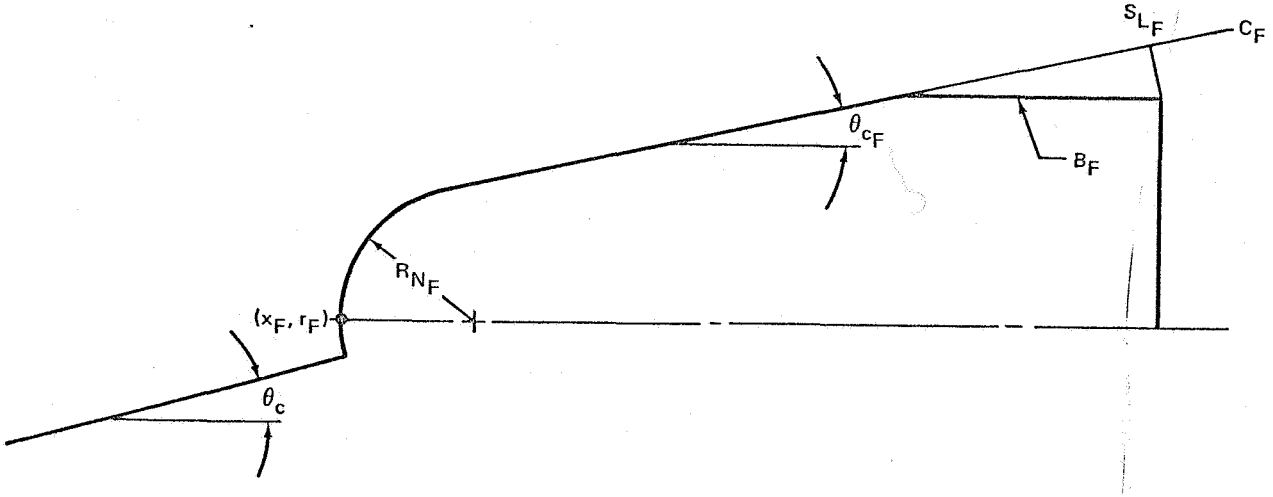

(b) FLARE GEOMETRY

Figure 4-1. Forebody and Flare Input Geometry Options

4.2 SHOCK LAYER STARTING SOLUTION

To generate initial values of the flow properties at the network points, the following procedure is followed. For a given body geometry, a modified Newtonian solution is obtained at the body surface. A linear interpolation is then made between the resulting surface values of flow properties and free-stream flow properties which are assumed as initial postshock conditions. For an asymmetric case, these data are repeated in each ϕ-plane, i.e., the initial data are always axisymmetric. The shock layer is initially set at a constant thickness, $\varepsilon_o = (F-f)_o$, up to the point where $\theta_B < \sin^{-1}(2/M_\infty)$. Beyond this point, $(F-f)_\ell = (F-f)_{\ell-1} + (2\Delta s_\ell)/M_\infty$ to ensure that the shock slope exceeds the free-stream Mach angle by a reasonable margin.

4.3 STABILITY CRITERION

Applying the conventional one-dimensional form of the stability condition on Δt in the three coordinate directions, one obtains the requirement that

$$\Delta t \leqq \bar{C} \left\{ \min \left[\frac{\left(1 + \frac{n}{R}\right)\Delta s}{|v_s| + \alpha}, \frac{\Delta n}{|v_n| + \alpha}, \frac{r d\phi}{|v_\phi| + \alpha} \right] \right\} \tag{4-1}$$

where $0 < \bar{C} \leqq 1$ is an input factor which is used when the linear stability criterion fails. During the calculation, the minimum Δt in the network is located, multiplied by $\bar{C}$ and assigned as the magnitude of the time step.

4.4 COMPUTATIONAL PROCEDURE

An idealized schematic of the forebody computational procedure is shown in Figure 4-2. A similar procedure is followed for the flare calculation with the addition of an interpolation subroutine for determining conditions immediately upstream of the portion of the flare shock wave contained within the forebody shock layer (see Appendix D for details). The special axis relations, which, for simplicity, are not explicitly identified in Figure 4-2, are omitted in the flare calculation because r_F is always greater than zero.

The structure of the program has been designed to facilitate modifications of the numerical procedures employed. In addition, the program makes efficient use of the computer core storage capacity to avoid time-consuming

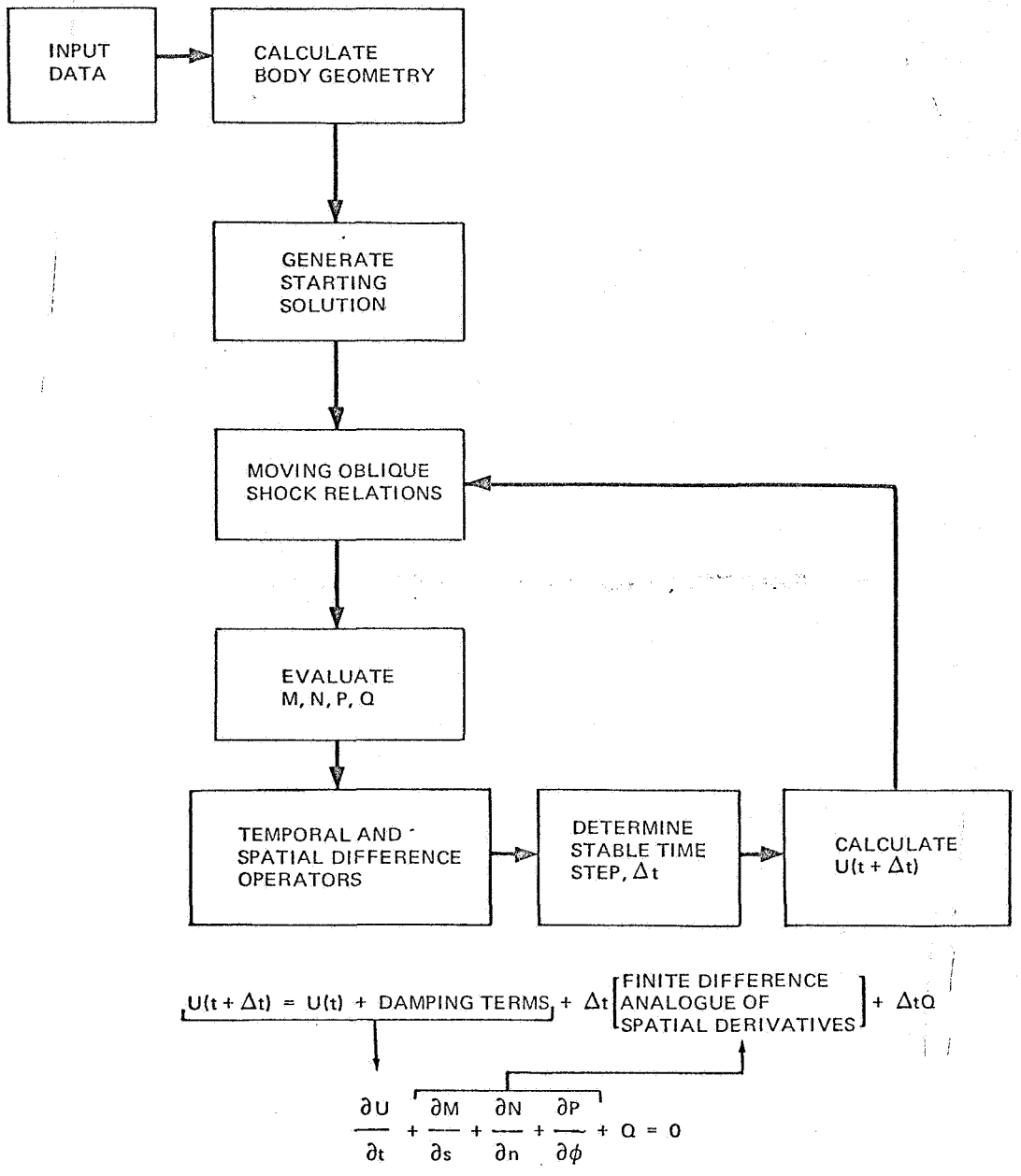

Figure 4-2. Idealized Schematic of Forebody Computational Procedure

tape handling operations. Although this requirement is a stringent one with respect to, for example, the number of network points which can be specified, the flow about some practical configurations at incidence to a free stream can be adequately described (subject to the condition that the calculations are stable with increasing time).

Section 5
NUMERICAL RESULTS

A series of test cases have been run to establish the operational capabilities of the program. Before proceeding to three-dimensional examples, symmetric flow cases were checked for consistency against both experimental and theoretical results.

5.1 ACCURACY AND UNIQUENESS OF BLUNT NOSE CALCULATIONS

Using the program as a blunt-body method, shock layer data were obtained for supersonic flow about a sphere at Mach numbers of approximately 3, 4, and 5. The exact Mach numbers used (2.996, 3.975, and 4.926) correspond to the available experimental data. The calculated shock detachment distance at the axis (Figure 5-1) and the surface pressure distributions (Figure 5-2)

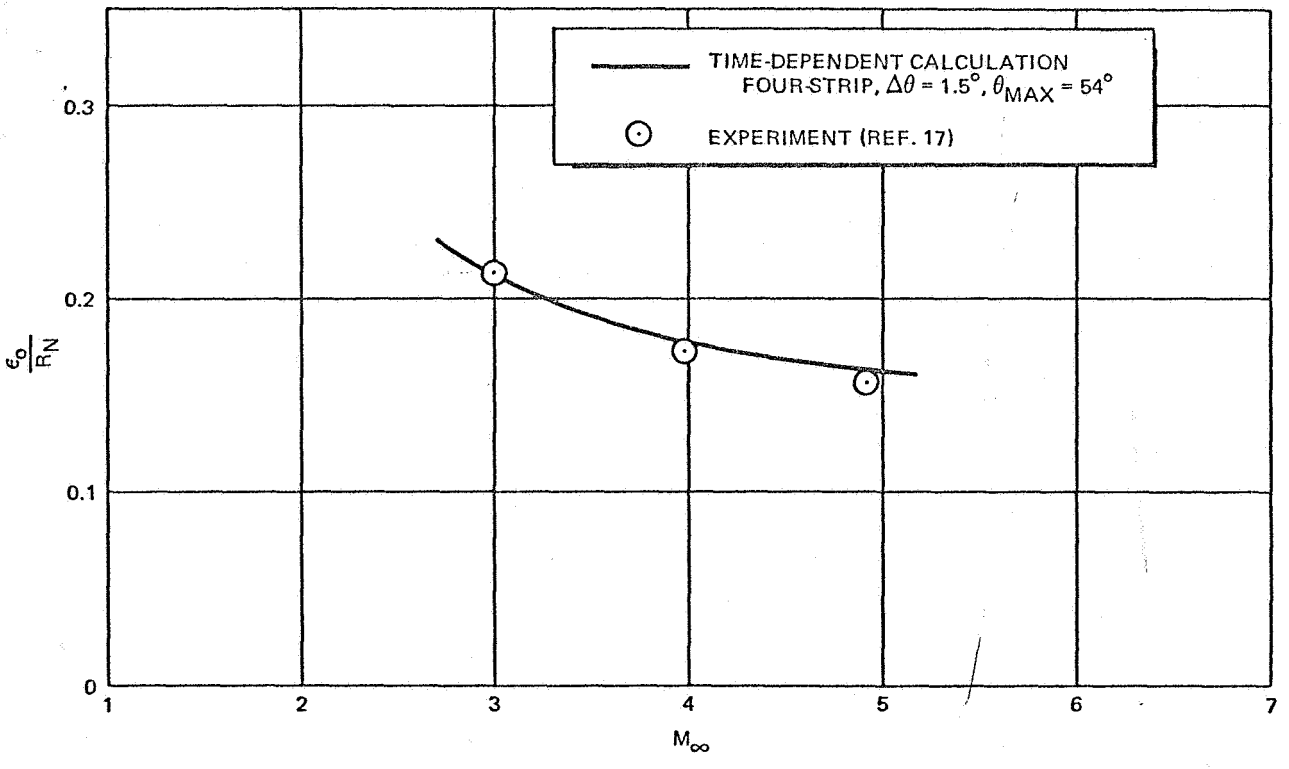

Figure 5-1. Shock Detachment Distance--Sphere

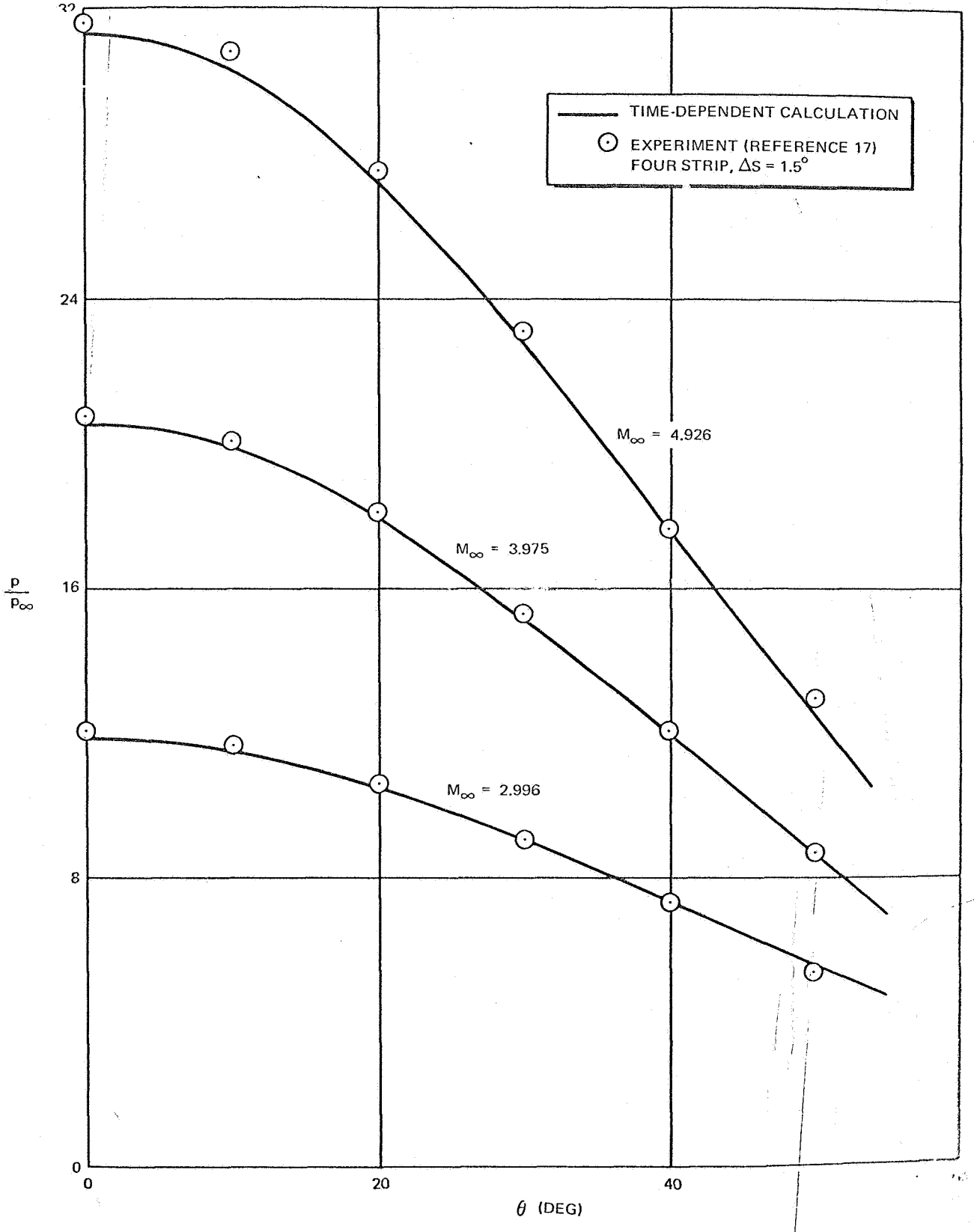

Figure 5-2. Surface Pressure Distribution – Sphere

are in reasonable agreement with experimental results when a four strip, $\Delta s = 1.5°$, mesh array is employed. For a given network of points, no significant change in converged results was obtained when the initial location of the bow shock was varied by a factor of two; this result is crucial because it supports the uniqueness of the calculations. The principal difficulty encountered during the sphere calculations was the inability to obtain valid, converged results at higher Mach numbers. Insufficient data have been obtained to establish the nature of this difficulty.

5.2 MESH SIZE DEPENDENCE

Unlike most blunt-body methods, the present time-dependent technique does not automatically establish stagnation point flow property values as those corresponding to passage through a normal shock wave followed by isentropic compression to the body surface (assuming symmetric flow). Further it has been generally noted that the rate of approach of flow property values to their steady-state limits is slowest near the body with surface density being a particularly sensitive variable in this respect. An examination of the behavior of the solution in the neighborhood of the stagnation point, therefore, affords a critical test for establishing flow field accuracy.

The test case chosen was a sphere with a fixed free-stream Mach number of 4. Referring to Figure 5-3, a reduction of the Δs increment from 6° to 1.5° with the number of shock layer strips increasing from two to four for the latter case results in acceptable stagnation values of pressure, density and detachment distance. In contrast to the floating mesh results of Reference 10 (which uses a different conditionally stable finite difference scheme), use of special axis relations appears to lead to less accurate results in the present program relative to results obtained by straddling the axis of symmetry with the finite difference network. Unfortunately, for the asymmetric flow case ($\alpha > 0$), the latter technique is not applicable since necessary symmetry conditions are lost.

The economic aspects of varying mesh size are indicated in Table 5-1 in terms of the computing time (Fortran IV, UNIVAC 1108) necessary to obtain converged answers (the average compilation time for the program of 11 sec is included).

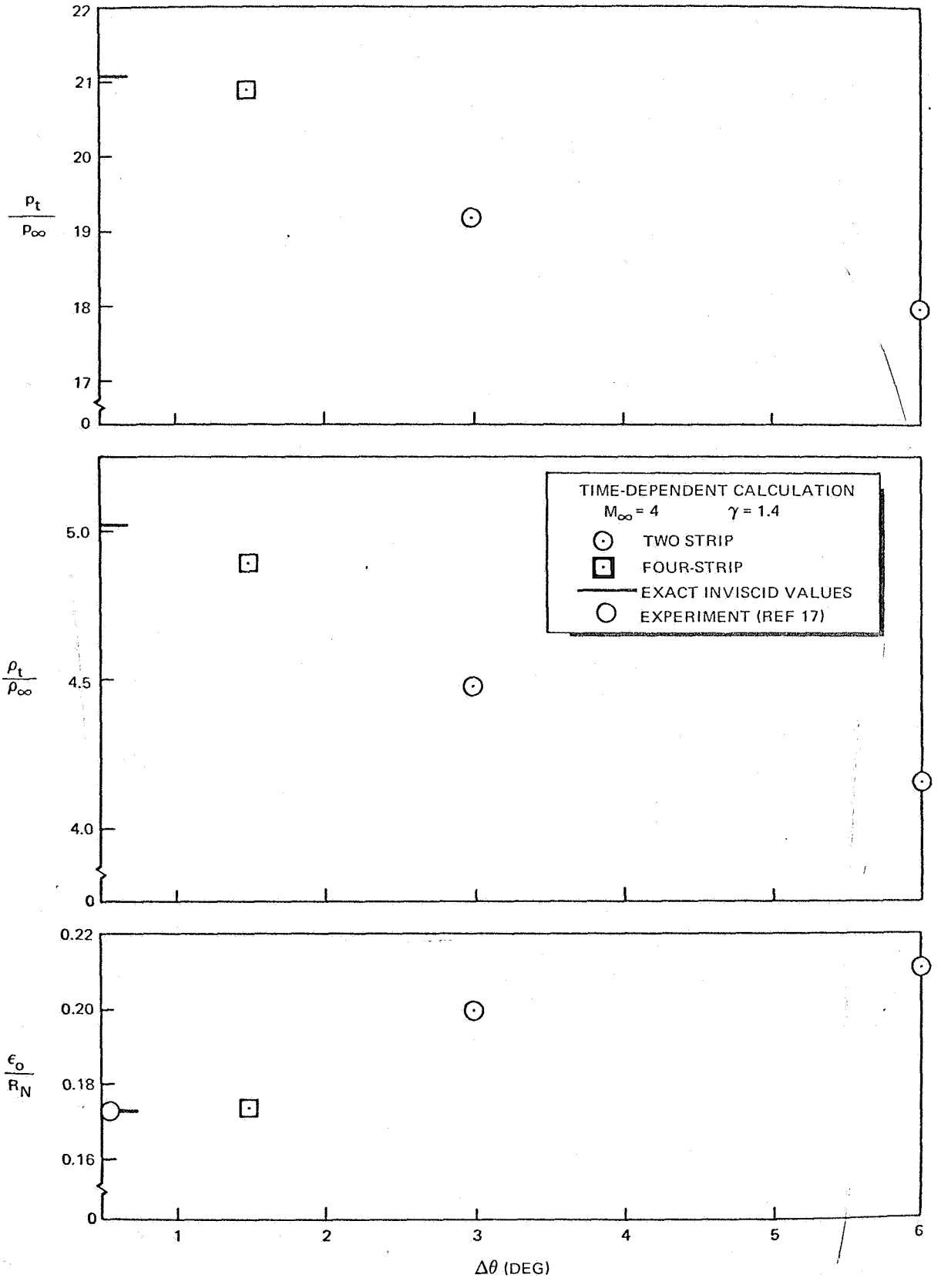

Figure 5-3. Effect of Mesh Dimensions on Sphere Stagnation Point Results

Table 5-1

MESH SIZE VARIATION

Δs	No. of Strips	No. of Time Cycles	$\left\|(dF/dt)_o\right\|$	Computing Time
1.5°	4	600	0.0002	3 min, 57sec
3°	2	400	0.0004	1 min, 8 sec
6°	2	400	0.000009	49 sec

5.3 EMPIRICAL ASPECTS OF STABILITY CRITERION

A time step factor, denoted by $\bar{C}$, has been previously identified in the definition of the stability condition on t, i.e., $(\Delta t)_{actual} = \bar{C}(\Delta t)_{linear}$, $0 < \bar{C} \leq 1$. It was found necessary in a large number of the cases described in this section to employ values of $\bar{C}$ ranging from 0.8 to 0.4 to effect a stable computation leading to valid asymptotic results. The linear Δt predictions used in the program are based upon application of one-dimensional concepts; therefore, it is likely that a more conservative estimate based on three-dimensional theory could be established which could reduce the dependence on empirical constants.

Certain characteristic behavior in the time varying flow field was noted as being indicative of the onset of instability. In particular, the appearance of alternating signs of dF/dt leading to a corrugated shock shape was an easily detectable instability mode. It must be emphasized that in some cases, an attempt to force stable behavior through extreme reduction of Δt (for example, use of $\bar{C} < 0.2$) can lead to anomalous flow field results. Because total energy E and total enthalpy, h_t, must approach steady-state values which are only a function of free stream conditions, these properties, which are monitored throughout the field, were a useful measure of the validity of the converged flow field data.

5.4 SPHERICALLY BLUNTED CONE COMPUTATIONS

The flow field about a blunted cone with a semi-apex angle of 24° was successfully calculated employing a two strip, $\Delta s = 6°$ network. The

initial and final bow shock positions are shown in Figure 5-4. Use of a constant Δs increment limited the overall length of the body to $x/R_N \cong 3$. The results exhibit qualitatively correct trends but are not particularly accurate since a coarse mesh was employed. The value of the coordinate system base radius of curvature, R, at the sphere-cone junction was set at both unity and "infinity" (10^{10}) corresponding, respectively, to either the sphere or cone values in order to estimate the effect of a curvature discontinuity on the calculations. A 10% deviation in downstream shock layer thickness was noted between the two cases. Use of a coordinate system base surface with continuous slope and radius of curvature may eliminate this perturbation.

A serious limitation in the operational range of the program was encountered when attempting to treat a hemisphere-cylinder. Flow properties, particularly pressure and density, on the afterbody surface displayed a consistent, unstable tendency to decrease rapidly during the time dependent process and eventually attain negative values. This behavior was later noted for several sphere-cone cases involving values of $\theta_C < 20°$. Decreasing Δs

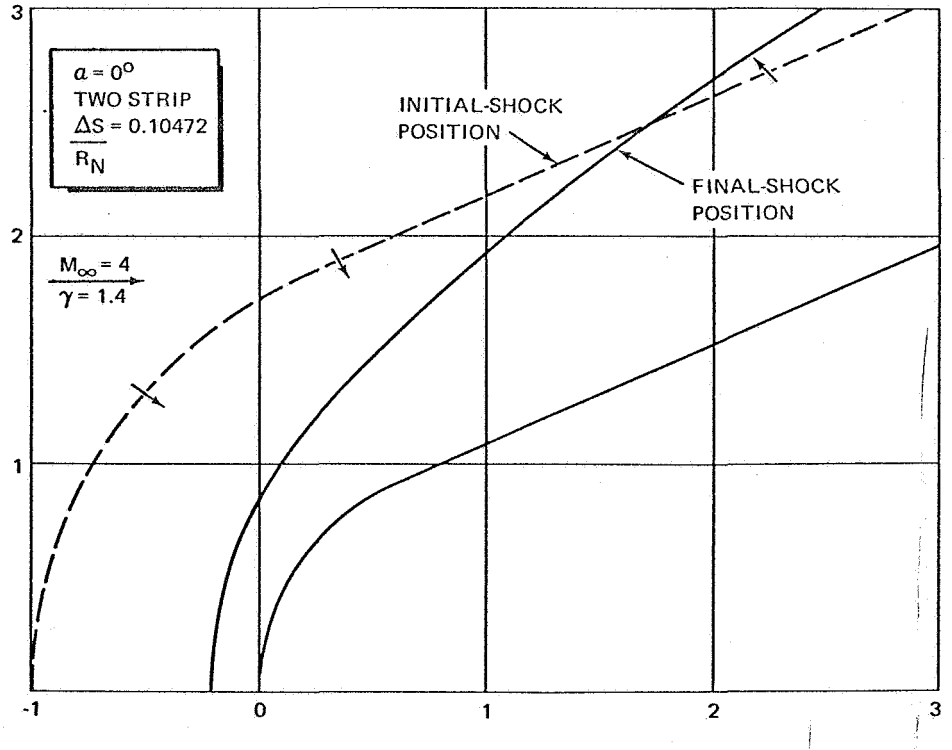

Figure 5-4. Time Dependent Calculation Blunted Cone ($\theta_C = 24°$)

through use of a special deck which eliminated ϕ-plane storage in favor of increased s-plane storage capacity did not correct this situation.

The variable Δs option which is intended to treat long afterbodies while maintaining small mesh intervals in the nose region was tested on the 24° blunted cone. A previous variable Δs scheme involving a doubling of the step size at intervals along the body was found to be unstable. The present scheme increases successive Δs steps by a geometric factor near unity, e.g., D = 1.05. A stable calculation was attained; however, a significant perturbation in nose region results could be noted, e.g., the bow shock was displaced outward (an examination of the literature on application of time dependent techniques to flow field problems indicates an emphasis on blunt configurations with minimal afterbody lengths).

5.5 ANGLE-OF-ATTACK COMPUTATIONS

The initial attempt to utilize the three-dimensional capabilities of the program involved a sphere calculation with the coordinate system axis of symmetry set at 6° incidence to the free stream. A reasonable check on the program was established as the resulting flow field was approximately symmetric about an axis parallel to the free stream direction and the rotated data corresponded to a conventional sphere solution. Small deviations from an exact match of $\alpha = 0°$ and rotated $\alpha = 6°$ values could possibly be attributed to perturbations arising from the asymmetry of damping terms associated with the axis relations and the restriction to a maximum of 9 ϕ-planes.

The previously described 24° sphere-cone configuration was successfully run at 6° angle of attack using 9 ϕ-planes. Examination of the circumferential variation of shock layer thickness (Figure 5-5) at four stations along the body indicates smooth, physically realistic trends from windward ($\phi = \pi$) to leeward ($\phi = 0$) planes. No tendency towards unstable behavior as a result of the three-dimensional nature of the calculations was noted. The computing time for this case was approximately nine minutes which should compare favorably with other three-dimensional techniques.

5.6 FLARE CALCULATIONS

The validity of the flare calculations was tested by computing a sequence of hemi-cylindrical flare cases considering a uniform oncoming stream, a

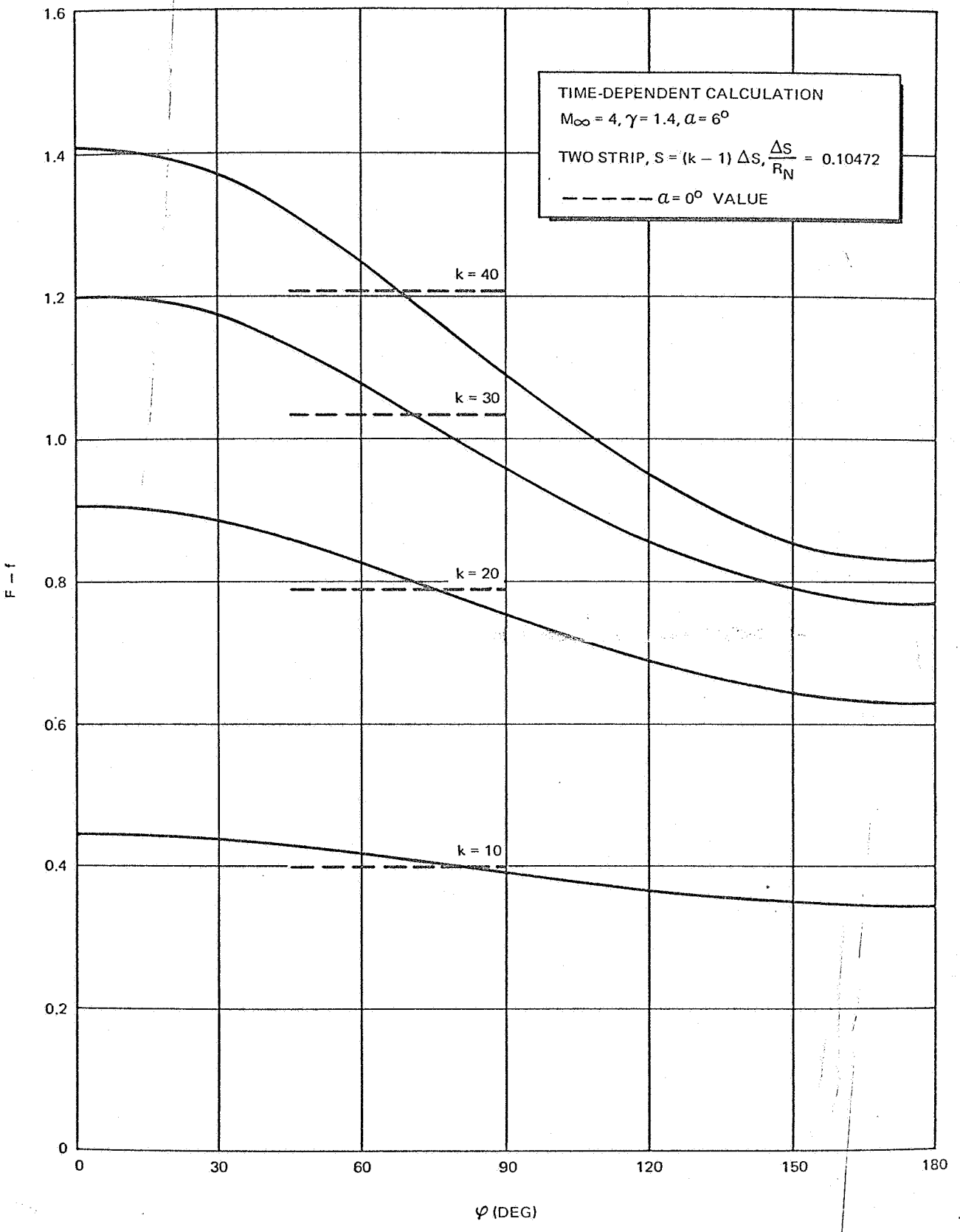

Figure 5-5. Blunted Cone at Angle of Attack – Circumferential Shock Layer Thickness

cylindrical forebody and varying flare radius. The resulting data should be bounded by sphere results as $r_F \to 0$ and two-dimensional cylinder results as $r_F \to \infty$. Examination of Figure 5-6 indicates that correct trends are exhibited when considering the variation of shock detachment distance with r_F. The rate of convergence of the flare case was less than a comparable forebody case in that more time steps were required to attain a given value of dF/dt.

At the time of preparation of this report, the fully coupled forebody-flare version of the program was nearing operational status.

5.7 CONVEX CORNERS

An initial attempt to compute a sphere-cone-cylinder case was unsuccessful. A critical examination of the effect of the corner on the stability of the calculations for this case was complicated by the previously established instability noted for afterbodies having small or zero slope.

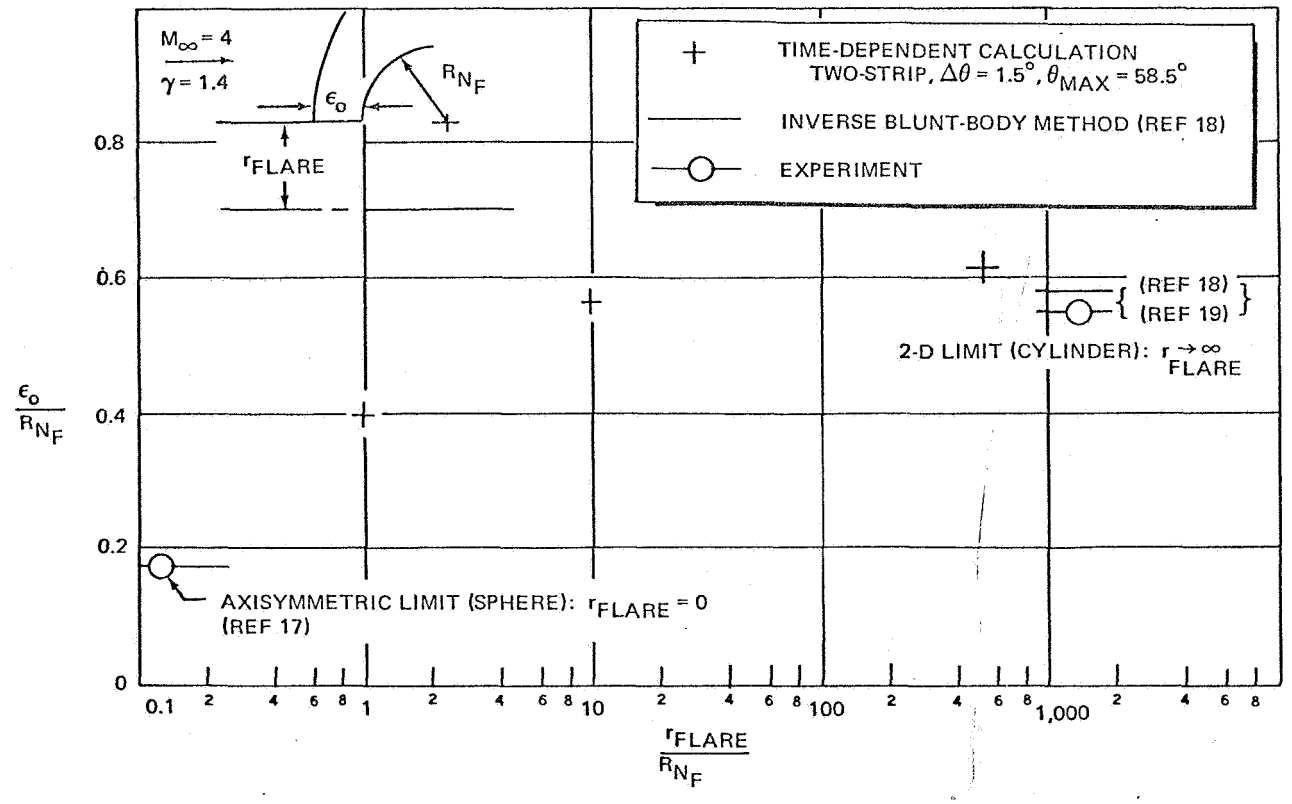

Figure 5-6. Shock Detachment Distance--Hemicylindrical Flare in Uniform Stream

Section 6
CONCLUSIONS

The principal objective of the present study has been to formulate and mechanize a practical three-dimensional flow field method by taking advantage of the recent advances in time-dependent computational techniques. To arrive at an economically feasible computing method, attention has been restricted to a floating mesh approach to reduce data storage requirements associated with the flow field description. The summary of results presented in the preceding section must be regarded in the nature of a progress report which describes both firm accomplishments and preliminary trends. The most encouraging observation is that the three-dimensional mode of calculation does not appear to introduce unstable behavior in cases which can be run successfully at zero angle of attack. In addition, the successful uniform stream flare calculation is a unique result.

While the difficulties associated with body slope discontinuities were anticipated, the nature of the instability mechanism present in afterbody calculations is less obvious. An in-depth study of this particular aspect of the problem using a modified numerical procedure such as the two-step Lax-Wendroff method is recommended owing to the present limitations on the operational range of the program.

REFERENCES

1. J. vonNeumann and R. D. Richtmeyer. A Method for the Numerical Calculation of Hydrodynamic Shocks. Journal of Applied Physics, Vol. 21, March 1950, Pages 232 - 237.
2. R. D. Richtmeyer and K. W. Morton. Difference Methods for Initial Value Problems. Interscience Publishers, John Wiley & Sons, New York, 1967.
3. H. L. Brode. Numerical Solutions of Spherical Blast Waves. The Rand Corporation, Report No. RM-1363-AEC, 29 September 1964.
4. A. A. Amsden. The Particle-in-Cell Method for the Calculation of the Dynamics of Compressible Fluids. Los Alamos Scientific Laboratory, Report No. LA-3466, February 1966.
5. I. O. Bohachevsky and R. E. Mates. A Direct Method for Calculation of the Flow About an Axisymmetric Blunt Body at Angle of Attack. American Institute of Aeronautics and Astronautics Journal, Vol. 4, No. 5, May 1966, Pages 776 - 782.
6. S. K. Godunov, A. V. Zabrodin, and G. P. Prokopov. A Computational Scheme for Two-Dimensional Nonstationary Problems of Gasdynamics and Calculation of the Flow from a Shock Wave Approaching a Stationary State. USSR J. Comp. Math. and Math. Phys. (Translation), 1961, Pages 1187 - 1219.
7. I. I. Babenko, G. P. Voskresenkii, A. N. Lyubinov, and V. V. Rusanov. Three Dimensional Flows of an Ideal Gas Past Smooth Bodies. NASA Report No. F-380 (Translation), April 1966.
8. G. Moretti and G. Bleich. Three-Dimensional Flow Around Blunt Bodies. American Institute of Aeronautics and Astronautics Journal, Vol. 5, No. 9, September 1967, Pages 1557 - 1562.
9. P. D. Lax and B. Wendroff. Difference Schemes with High Order of Accuracy for Solving Hyperbolic Equations. AEC Computing and Applied Mathematics Center, Courant Institute of Mathematical Sciences Report No. NYO-9759, July 1962.
10. B. S. Masson. Two-Dimensional Flow Field Calculations by the Godunov Method. Aeronutronic Report No. U-4137, July 1967.
11. L. Crocco. A Suggestion for the Numerical Solution of the Steady Navier-Stokes Equations. American Institute of Aeronautics and Astronautics Journal, Vol. 3, No. 10, 1965, Pages 1824 - 1832.

12. R. J. Hakkinen. Supersonic Flow Near Two-Dimensional and Axially Symmetric Convex Corners and Curvature Discontinuities. Douglas Report No. SM-27747, July 1958.

13. R. Vaglio-Laurin. Transonic Rotational Flow over a Convex Corner. Journal of Fluid Mechanics, Vol. 9, Part 1, 1960, Pages 81 - 103.

14. O. M. Belotserkovskii. Flow over Blunt Bodies in a Supersonic Free Stream. Computing Center, Academy of Sciences, Moscow, 1967.

15. W. F. Ames (Editor). Nonlinear Partial Differential Equations. Academic Press, New York, 1967.

16. P. D. Lax. Weak Solutions of Nonlinear Hyperbolic Equations and Their Numerical Computations. Communications on Pure and Applied Mathematics, Vol. 7, 1954, Pages 159 - 193.

17. J. Xerikos and W. A. Anderson. An Experimental Investigation of the Shock Layer Surrounding a Sphere in Supersonic Flow. AIAA Journal, Vol. 3, No. 3, March 1965.

18. R. A. Batchelder. An Inverse Method for Inviscid Ideal Gas Flow Fields Behind Analytic Shock Shapes. Douglas Report No. SM-42588, July 1963.

19. W. D. Hayes and R. F. Probstein. Hypersonic Flow Theory: Volume I. Inviscid Flows. Academic Press, New York, 1966, Page 419.

Appendix A

DERIVATION OF GOVERNING EQUATIONS IN GENERAL ORTHOGONAL CURVILINEAR COORDINATES

The equations expressing conservation of mass, momentum, and energy for the unsteady motion of an inviscid, nonheat conducting fluid are given below in Eulerian form.

$$\text{(continuity)} \quad \frac{\partial \rho}{\partial t} + \nabla \cdot \rho \vec{V} = 0 \tag{A-1}$$

$$\text{(momentum)} \quad \frac{\partial \vec{V}}{\partial t} + \nabla \left(\frac{V^2}{2} \right) - \vec{V} \times (\nabla \times V) + \frac{1}{\rho} \nabla p = 0 \tag{A-2}$$

$$\text{(energy)} \quad \frac{\partial E}{\partial t} + \vec{V} \cdot \nabla \left(E + \frac{p}{\rho} \right) - \frac{p}{\rho^2} \frac{\partial \rho}{\partial t} = 0 \tag{A-3}$$

where, denoting dimensional quantities with a bar,

$$\rho = \frac{\bar{\rho}}{\rho_\infty} = \text{density}$$

$$p = \frac{\bar{p}}{\rho_\infty V_\infty^2} = \text{pressure}$$

$$V = \frac{\bar{V}}{V_\infty} = \text{total velocity}$$

$$E = \frac{\bar{E}}{V_\infty^2} = \text{specific total energy}$$

The energy equation for unsteady adiabatic flow may also be expressed in terms of the specific total enthalpy, h_t, of the fluid:

$$\frac{dh_t}{dt} = \left(\frac{\partial}{\partial t} + V \cdot \nabla \right) h_t = \frac{1}{\rho} \frac{\partial p}{\partial t}$$

where

$$h_t = h + \frac{1}{2} V^2 = E + \frac{p}{\rho}$$

since

$$h = e + \frac{p}{\rho},$$

e = specific internal energy and

$$E = e + \frac{1}{2} V^2$$

For an adiabatic process involving a perfect gas (i. e., $p = \rho RT$; c_p, c_v = constant),

$$h = \frac{\gamma}{\gamma - 1} \frac{p}{\rho},$$

therefore,

$$E = \frac{1}{\gamma - 1} \frac{p}{\rho} + \frac{1}{2} V^2 \qquad \text{(A-4)}$$

Although the present study is restricted to consideration of a perfect gas, the extension of the analysis to treat a gas in thermodynamic equilibrium is straightforward and primarily involves the introduction of an empirical description of the required thermodynamic properties. In addition, certain explicit relationships, valid for the perfect gas case, will become implicit thus leading to iterative calculations with an attendant increase in computing time.

The governing equations will now be written in general curvilinear, orthogonal coordinates (α, β, γ) where

$$(ds)^2 = h_\alpha{}^2 (d\alpha)^2 + h_\beta{}^2 (d\beta)^2 + h_\gamma{}^2 (d\gamma)^2$$

and

$$\vec{V} = v_\alpha \vec{e}_\alpha + v_\beta \vec{e}_\beta + v_\gamma \vec{e}_\gamma$$

The basic operators required are given by

$$\nabla \cdot \vec{V} = \frac{1}{h_\alpha h_\beta h_\gamma}\left[\frac{\partial}{\partial\alpha}(h_\beta h_\gamma v_\alpha) + \frac{\partial}{\partial\beta}(h_\gamma h_\alpha v_\beta) + \frac{\partial}{\partial\gamma}(h_\alpha h_\beta v_\gamma)\right]$$

$$\nabla V = \frac{1}{h_\alpha}\frac{\partial V}{\partial_\alpha}\vec{e}_\alpha + \frac{1}{h_\beta}\frac{\partial V}{\partial\beta}\vec{e}_\beta + \frac{1}{h_\gamma}\frac{\partial V}{\partial\gamma}\vec{e}_\gamma\ ,\quad V = \left|\vec{V}\right|$$

$$\nabla \times \vec{V} = \xi\vec{e}_\alpha + \eta\vec{e}_\beta + \zeta\vec{e}_\gamma\ ,$$

$$\xi = \frac{1}{h_\beta h_\gamma}\left[\frac{\partial}{\partial\beta}(h_\gamma v_\gamma) - \frac{\partial}{\partial\gamma}(h_\beta v_\beta)\right]$$

$$\eta = \frac{1}{h_\gamma h_\alpha}\left[\frac{\partial}{\partial\gamma}(h_\alpha v_\alpha) - \frac{\partial}{\partial\alpha}(h_\gamma v_\gamma)\right]$$

$$\zeta = \frac{1}{h_\alpha h_\beta}\left[\frac{\partial}{\partial\alpha}(h_\beta v_\beta) - \frac{\partial}{\partial\beta}(h_\alpha v_\alpha)\right]$$

$$(\nabla \times \vec{V}) \times \vec{V} = (v_\gamma\eta - v_\beta\zeta)\vec{e}_\alpha + (v_\alpha\zeta - v_\gamma\xi)\vec{e}_\beta + (v_\beta\xi - v_\alpha\eta)\vec{e}_\gamma$$

Application of these operators to Equations A-1, A-2, and A-3 yields

Continuity:

$$h_\alpha h_\beta h_\gamma \frac{\partial\rho}{\partial t} + \frac{\partial}{\partial\alpha}(h_\beta h_\gamma \rho v_\alpha) + \frac{\partial}{\partial\beta}(h_\gamma h_\alpha \rho v_\beta) + \frac{\partial}{\partial\gamma}(h_\alpha h_\beta \rho v_\gamma) = 0 \qquad \text{(A-5)}$$

Momentum

α direction:

$$\frac{\partial v_\alpha}{\partial t} + \frac{1}{h_\alpha}\frac{\partial}{\partial\alpha}\left(\frac{V^2}{2}\right) + (v_\gamma\eta - v_\beta\zeta) + \frac{1}{h_\alpha}\frac{1}{\rho}\frac{\partial p}{\partial\alpha} = 0 \qquad \text{(A-6)}$$

β direction:

$$\frac{\partial v_\beta}{\partial t} + \frac{1}{h_\beta}\frac{\partial}{\partial\beta}\left(\frac{V^2}{2}\right) + (v_\alpha\zeta - v_\gamma\xi) + \frac{1}{h_\beta}\frac{1}{\rho}\frac{\partial p}{\partial\beta} = 0 \qquad \text{(A-7)}$$

γ direction:

$$\frac{\partial v_\gamma}{\partial t} + \frac{1}{h_\gamma}\frac{\partial}{\partial\gamma}\left(\frac{V^2}{2}\right) + (v_\beta\xi - v_\alpha\eta) + \frac{1}{h_\gamma}\frac{1}{\rho}\frac{\partial p}{\partial\gamma} = 0 \qquad \text{(A-8)}$$

Energy:

$$\frac{\partial E}{\partial t} + \frac{v_\alpha}{h_\alpha}\frac{\partial}{\partial \alpha}\left(E + \frac{p}{\rho}\right) + \frac{v_\beta}{h_\beta}\frac{\partial}{\partial \beta}\left(E + \frac{p}{\rho}\right) + \frac{v_\gamma}{h_\gamma}\frac{\partial}{\partial \gamma}\left(E + \frac{p}{\rho}\right) - \frac{p}{\rho^2}\frac{\partial \rho}{\partial t} = 0 \qquad (A\text{-}9)$$

The governing equations will now be written in conservation-law form, i. e.,

$$\frac{\partial \bar{U}}{\partial t} + \frac{\partial \bar{M}}{\partial \alpha} + \frac{\partial \bar{N}}{\partial \beta} + \frac{\partial \bar{P}}{\partial \gamma} + Q = 0$$

where $\bar{U}$ can represent mass, components of momentum in the coordinate directions, or energy. The momentum and energy equations assume this form when properly combined with the continuity equation. For example, the operation $h_\alpha h_\beta h_\gamma \rho$ x (α - momentum equation) + v_α x (continuity equation) yields the expression describing conservation of the α - component of momentum. Following a similar procedure for the remaining equations, $\bar{U}$, $\bar{M}$, $\bar{N}$, $\bar{P}$, and Q are given by

$$\bar{U} = h_\alpha h_\beta h_\gamma \begin{bmatrix} \rho \\ \rho v_\alpha \\ \rho v_\beta \\ \rho v_\gamma \\ \rho E \end{bmatrix}, \quad \bar{M} = h_\beta h_\gamma \begin{bmatrix} \rho v_\alpha \\ \rho v_\alpha^2 + p \\ \rho v_\alpha v_\beta \\ \rho v_\alpha v_\gamma \\ \rho v_\alpha \left(E + \frac{p}{\rho}\right) \end{bmatrix}, \quad \bar{N} = h_\gamma h_\alpha \begin{bmatrix} \rho v_\beta \\ \rho v_\beta v_\alpha \\ \rho v_\beta^2 + p \\ \rho v_\beta v_\gamma \\ \rho v_\beta \left(E + \frac{p}{\rho}\right) \end{bmatrix}$$

$$\bar{P} = h_\gamma h_\beta \begin{bmatrix} \rho v_\gamma \\ \rho v_\gamma v_\alpha \\ \rho v_\gamma v_\beta \\ \rho v_\gamma^2 + p \\ \rho v_\gamma (E + p/\rho) \end{bmatrix},$$

$$
Q = \begin{bmatrix}
0 \\
\rho v_\alpha \left(h_\gamma v_\beta \frac{\partial h_\alpha}{\partial \beta} + h_\beta v_\gamma \frac{\partial h_\alpha}{\partial \gamma} \right) - h_\gamma \left(\rho v_\beta{}^2 + p \right) \frac{\partial h_\beta}{\partial \alpha} - h_\beta \left(\rho v_\gamma{}^2 + p \right) \frac{\partial h_\gamma}{\partial \alpha} \\
\rho v_\beta \left(h_\alpha v_\gamma \frac{\partial h_\beta}{\partial \gamma} + h_\gamma v_\alpha \frac{\partial h_\beta}{\partial \alpha} \right) - h_\alpha \left(\rho v_\gamma{}^2 + p \right) \frac{\partial h_\gamma}{\partial \beta} - h_\gamma \left(\rho v_\alpha{}^2 + p \right) \frac{\partial h_\alpha}{\partial \beta} \\
\rho v_\gamma \left(h_\beta v_\alpha \frac{\partial h_\gamma}{\partial \alpha} + h_\alpha v_\beta \frac{\partial h_\gamma}{\partial \beta} \right) - h_\beta \left(\rho v_\alpha{}^2 + p \right) \frac{\partial h_\alpha}{\partial \gamma} - h_\alpha \left(\rho v_\beta{}^2 + p \right) \frac{\partial h_\beta}{\partial \gamma} \\
0
\end{bmatrix}
$$

For a rectangular Cartesian coordinate system $\{x, y, z\}$, the transformation scale factors h_α, h_β, and h_γ become unity and $Q \equiv 0$. The present study considers a three-dimensional orthogonal curvilinear coordinate system $\{s, n, \phi\}$ where s and n are coordinates along and normal to, respectively, an axisymmetric surface described, for convenience, in cylindrical polar coordinates $\{x, r, \varphi\}$. The circumferential angle, ϕ, is measured in a plane normal to the x-axis (see Figure A-1). The relationship between the $\{s, n, \phi\}$ and $\{x, r, \varphi\}$ systems is given by

$$
\left.
\begin{aligned}
x &= x_o(s) - n \sin\theta(s) && \text{(a)} \\
r &= r_o(s) + n \cos\theta(s) && \text{(b)} \\
\varphi &= \phi && \text{(c)}
\end{aligned}
\right\} \qquad \text{(A-10)}
$$

where θ is the angle between the x-axis and a tangent to the reference surface S lying in a circumferential plane defined by ϕ = constant.

The transformation scale factors for the curvilinear system become

$$
\begin{aligned}
h_\alpha &= h_s = 1 + \frac{n}{R}, \quad R = R(s) = -\left(\frac{\partial \theta}{\partial s} \right)^{-1} \\
h_\beta &= h_n = 1 \\
h_\gamma &= h_\phi = r
\end{aligned}
\qquad \text{(A-11)}
$$

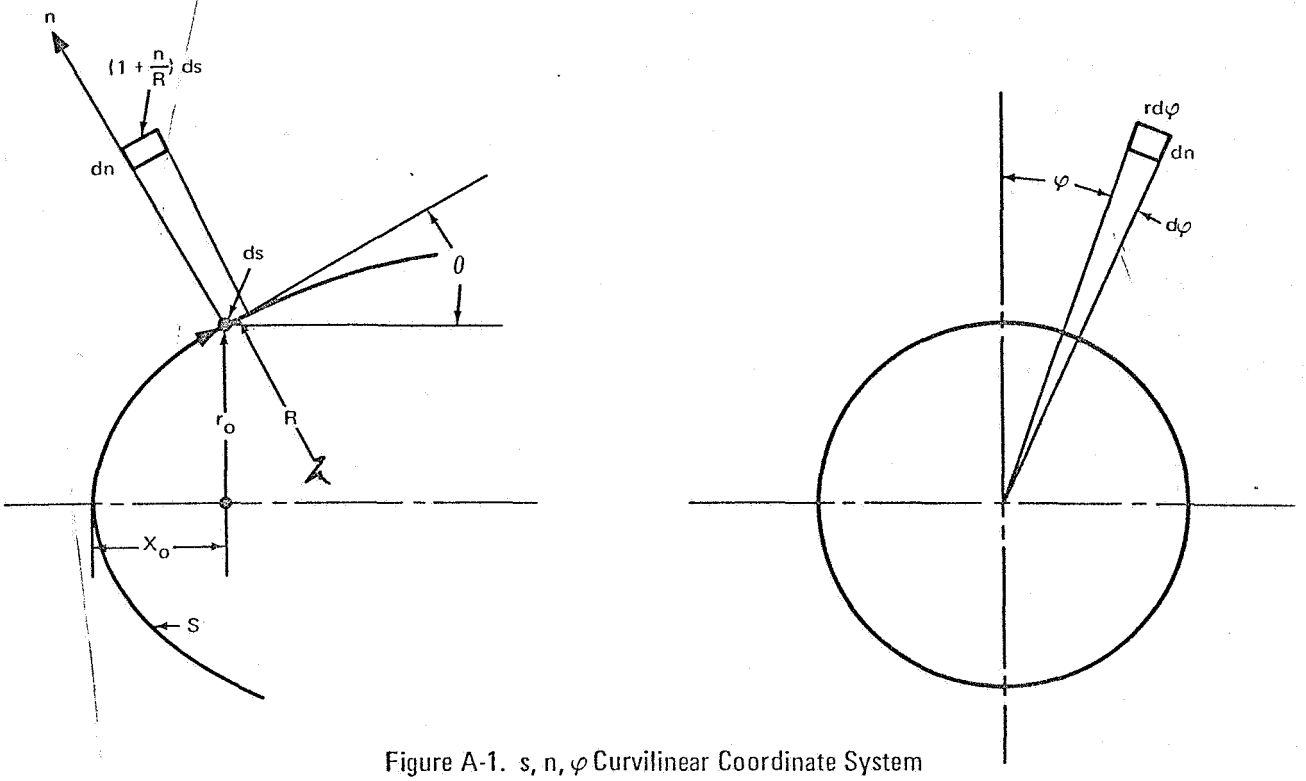

Figure A-1. s, n, φ Curvilinear Coordinate System

Evaluation of Q(s, n, ϕ) requires determination of the partial derivatives of the transformation scale factors with respect to the coordinates, i. e., determination of the matrix operator given by

$$J\left(\frac{h_\alpha,\ h_\beta,\ h_\gamma}{\alpha,\ \beta,\ \gamma}\right) \qquad \begin{pmatrix} \frac{\partial h_\alpha}{\partial \alpha} & \frac{\partial h_\alpha}{\partial \beta} & \frac{\partial h_\alpha}{\partial \gamma} \\ \frac{\partial h_\beta}{\partial \alpha} & \frac{\partial h_\beta}{\partial \beta} & \frac{\partial h_\beta}{\partial \gamma} \\ \frac{\partial h_\gamma}{\partial \alpha} & \frac{\partial h_\gamma}{\partial \beta} & \frac{\partial h_\gamma}{\partial \gamma} \end{pmatrix}$$

Use of Equations A-10 and A-11 yields

$$J\left(\frac{h_s,\ h_n,\ h_\phi}{s,\ n,\ \phi}\right) = \begin{pmatrix} \frac{-n}{R^2}\frac{\partial R}{\partial s} & \frac{1}{R} & 0 \\ 0 & 0 & 0 \\ \sin\theta\ (1 + \frac{n}{R}) & \cos\theta & 0 \end{pmatrix}$$

Appendix B
DEVELOPMENT OF MOVING BOW AND FLARE SHOCK RELATIONS

The Rankine-Hugoniot shock relations will be derived in a form suitable for describing flow properties behind a moving three-dimensional shock surface. As before, velocities are normalized by V_∞, density by ρ_∞, and pressure by $\rho_\infty V_\infty^2$. This choice of nondimensionalization does not introduce constants into the equations, thus the equations retain their original form.

Initially, the shock geometry and the total velocity vector immediately upstream of the shock must be expressed in terms of the previously defined $\{s, n, \phi\}$ coordinate system.

B. 1 SHOCK GEOMETRY

Define the shock surface by the relation $g(s, n, \phi; t) = 0$. The normal to the surface is, therefore, given by

$$\nabla g(s, n, \phi; t) = \frac{1}{\left(1 + \frac{n}{R}\right)} \frac{\partial g}{\partial s} \vec{e}_s + \frac{\partial g}{\partial n} \vec{e}_n + \frac{1}{r} \frac{\partial g}{\partial \phi} \vec{e}_\phi$$

The unit normal becomes (Figure B-1)

$$\vec{N} = \frac{\nabla g}{G} = \cos\beta_s \vec{e}_s + \cos\beta_n \vec{e}_n + \cos\beta_\phi \vec{e}_\phi \qquad \text{(B-1)}$$

where

$$G = \left[\frac{1}{\left(1 + \frac{n}{R}\right)^2} \left(\frac{\partial g}{\partial s}\right)^2 + \left(\frac{\partial g}{\partial n}\right)^2 + \frac{1}{r^2} \left(\frac{\partial g}{\partial \phi}\right)^2 \right]^{\frac{1}{2}}$$

B. 2 UPSTREAM VELOCITY VECTOR

In order to resolve the total velocity vector immediately upstream of the bow or flare shock wave into components normal and tangential to the shock

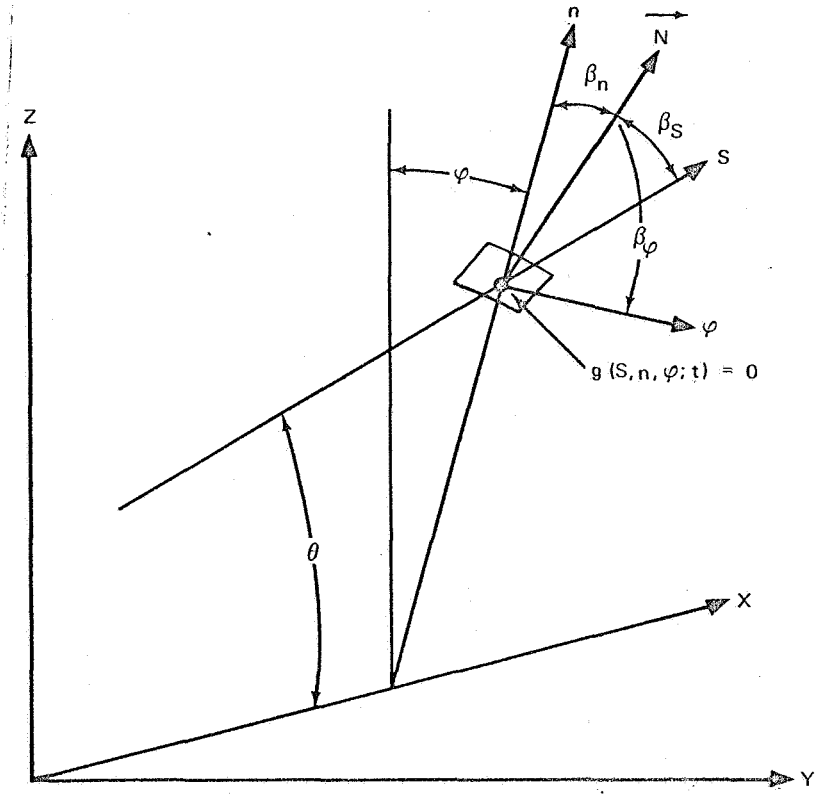

Figure B-1. Orientation of Normal to Shock Surface

surface, it is convenient to express the velocity vector in $\{s, n, \phi\}$ coordinates, coordinates, i. e.,

$$\vec{V} = v_{s_o}\vec{e}_s + v_{n_o}\vec{e}_n + v_{\phi_o}\vec{e}_\phi \qquad \text{(B-2)}$$

When treating the segment of the flare shock lying within the forebody shock layer, the nondimensional upstream components v_{s_o}, v_{n_o}, and v_{ϕ_o} are obtained through interpolation of data yielded by the converged forebody calculation. For the bow shock or portion of the flare shock beyond the bow-flare shock intersection point, free-stream conditions prevail; therefore, one obtains

$$\left.\begin{aligned} v_{s_o} &= v_{s_\infty} = \cos\alpha\cos\theta + \sin\alpha\sin\theta\cos\phi \\ v_{n_o} &= v_{n_\infty} = -\cos\alpha\sin\theta + \sin\alpha\cos\theta\cos\phi \\ v_{\phi_o} &= v_{\phi_\infty} = -\sin\alpha\sin\phi \end{aligned}\right\} \qquad \text{(B-3)}$$

The angle of attack, α, is measured between the free-stream velocity vector and the axis of symmetry of the vehicle. Because the present study is restricted to consideration of an axisymmetric vehicle at incidence, the flow field has a single plane of symmetry defined by the x-axis and the free-stream velocity vector.

The normal component of the upstream velocity is given by

$$V_{N_o} = \vec{V} \cdot \vec{N} = \frac{1}{G} \left[\frac{1}{\left(1 + \frac{n}{R}\right)} v_{s_o} \frac{\partial g}{\partial s} + v_{n_o} \frac{\partial g}{\partial n} + \frac{1}{r} v_{\phi_o} \frac{\partial g}{\partial \phi} \right] \tag{B-4}$$

As the tangential component, V_{T_o}, is conserved across the shock wave, V_{N_o}, ρ_o, p_o, and the shock velocity U_s can be introduced into the moving normal shock relations to determine postshock flow properties. Referring to Figure B-2, conservation of mass, normal momentum and energy across the shock are expressed by

$$\rho_o u_o = \rho_N u_N \tag{B-5}$$

$$p_o + \rho_o u_o^2 = p_N + \rho_N u_N^2 \tag{B-6}$$

$$\frac{\gamma}{\gamma - 1} \frac{p_o}{\rho_o} + \frac{1}{2} u_o^2 = \frac{\gamma}{\gamma - 1} \frac{p_N}{\rho_N} + \frac{1}{2} u_N^2 \tag{B-7}$$

Use of Equation B-7 restricts the remainder of the analysis to consideration of a perfect gas.

Introducing Equations B-5 and B-7 into Equation B-6 yields

$$u_N = \frac{2\gamma}{u_o(\gamma + 1)} \left(\frac{p_o}{\rho_o} + u_o^2 \right) - u_o$$

or, using $u_o = V_{N_o} - U_s$ and $u_N = V_N - U_s$,

$$V_N = \frac{2\gamma}{(V_{N_o} - U_s)(\gamma + 1)} \left[\frac{p_o}{\rho_o} + (V_{N_o} - U_s)^2 \right] - V_{N_o} + 2U_s \tag{B-8}$$

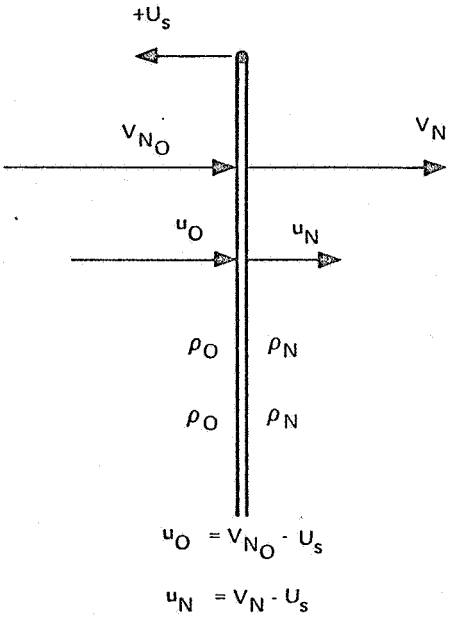

Figure B-2. Transformation Relations Between Moving and Stationary Shock Waves

Solving for the remaining postshock properties

$$\rho_N = \rho_o \left(\frac{V_{N_o} - U_s}{V_N - U_s} \right) \tag{B-9}$$

$$p_N = p_o + \rho_o (V_{N_o} - U_s)(V_{N_o} - V_N) \tag{B-10}$$

An expression for $U_s (\rho_N; p_o, \rho_o, V_{N_o})$ can be obtained through use of Equations B-8 and B-9:

$$U_s = \left[\frac{k (p_o / \rho_o)}{(\rho_o / \rho_N) - k + 1} \right]^{\frac{1}{2}} + V_{N_o}, \quad k = \frac{2\gamma}{\gamma + 1} \tag{B-11}$$

For uniform free-stream conditions ahead of the shock, Equations B-8 through B-11 become

$$V_N = \frac{2\gamma}{(V_{N_\infty} - U_s)(\gamma + 1)} \left[\frac{1}{\gamma M_\infty^2} + (V_{N_\infty} - U_s)^2 \right] - V_N + 2U_s \tag{B-12}$$

$$\rho_N = \frac{V_{N_\infty} - U_s}{V_N - U_s} \tag{B-13}$$

$$p_N = \frac{1}{\gamma M_\infty^2} + (V_{N_\infty} - U_s)(V_{N_\infty} - V_N) \tag{B-14}$$

$$U_s = \left[\frac{2/M_\infty^2}{(\gamma + 1)/\rho_N - (\gamma - 1)} \right]^{\frac{1}{2}} + V_{N_\infty} \tag{B-15}$$

Finally, the components of velocity behind the shock are given by

$$v_s = v_{s_o} + (V_N - V_{N_o}) \cos \beta_s \tag{B-16}$$

$$v_n = v_{n_o} + (V_N - V_{N_o}) \cos \beta_n \tag{B-17}$$

$$v_\phi = v_{\phi_o} + (V_N - V_{N_o}) \cos \beta_\phi \tag{B-18}$$

where

$$\cos \beta_s = \frac{1}{G\left(1 + \frac{n}{R}\right)} \frac{\partial g}{\partial s} \tag{B-19}$$

$$\cos \beta_n = \frac{1}{G} \frac{\partial g}{\partial n} \tag{B-20}$$

$$\cos \beta_\phi = \frac{1}{Gr} \frac{\partial g}{\partial \phi} \tag{B-21}$$

The description of postshock flow properties in terms of shock geometry, velocity, and upstream conditions is now complete.

Shock Relations at the Axis:

Define the shock surface by

$$g(s, n, \phi, t) = n - F(s, \phi, t) = 0 \qquad \text{(B-22)}$$

Then

$$\cos \beta_s = \frac{1}{G\left(1+\frac{F}{R}\right)} \left(-\frac{\partial F}{\partial s}\right)$$

$$\cos \beta_n = \frac{1}{G}$$

$$\cos \beta_\phi = \frac{1}{Gr} \left(-\frac{\partial F}{\partial \phi}\right)$$

$$G = \left[\frac{1}{\left(1+\frac{F}{R}\right)^2}\left(\frac{\partial F}{\partial s}\right)^2 + 1 + \frac{1}{\gamma_s^2}\left(\frac{\partial F}{\partial \phi}\right)^2\right]^{1/2}, \quad r_s = r_o + F\cos\theta$$

As $r_s \to 0$, $F \to F_o$ and $\partial F/\partial \phi \to 0$

Since F is a regular function in the neighborhood of $s = 0$

$$\lim_{s\to 0} \frac{\frac{\partial F}{\partial \phi}}{r_s} = \lim_{s\to 0} \frac{\frac{\partial}{\partial s}\left[\frac{\partial F}{\partial \phi}\right]}{\sin\theta\left(1+\frac{F}{R}\right)} = \frac{\left\{\frac{\partial}{\partial \phi}\left[\frac{\partial F}{\partial s}\right]\right\}_o}{\left(1+\frac{F_o}{R_o}\right)} \qquad \text{(B-23)}$$

In the $\phi = 0$ plane, $\left\{\frac{\partial}{\partial \phi}\left[\frac{\partial F}{\partial s}\right]\right\}_o = 0$ therefore, the geometric shock relations reduce to

$$\cos \beta_s = \frac{-\left(\frac{\partial F}{\partial s}\right)_o}{G_o\left(1+\frac{F_o}{R_o}\right)}, \quad G_o = \left[\frac{1}{\left(1+\frac{F_o}{R_o}\right)^2}\left(\frac{\partial F}{\partial s}\right)_o^2 + 1\right]^{1/2}$$

$$\cos \beta_n = \frac{1}{G_o}$$

$$\cos \beta_\phi = 0$$

(Note that $\beta_s = \pi/2 - \beta_n$ in this case.)

Appendix C
DERIVATION OF SPECIAL FORM OF GOVERNING EQUATIONS VALID AT THE AXIS OF SYMMETRY

The vehicle axis of symmetry which coincides with the x-axis is a regular line of the flow field and a singular line of the (s, n, ϕ)-coordinate system. A limiting form of the governing equations must therefore be derived which does not display singular behavior as $r \to 0$. The conservation-law form of the equations was previously given by Equation 2-1 as

$$\frac{\partial \overline{U}}{\partial t} + \frac{\partial \overline{M}}{\partial s} + \frac{\partial \overline{N}}{\partial n} + \frac{\partial \overline{P}}{\partial \phi} + Q = 0$$

or

$$\frac{\partial}{\partial t}\left[r\left(1 + \frac{n}{R}\right) U\right] + \frac{\partial}{\partial s}\left[rM(U)\right] + \frac{\partial}{\partial n}\left[r\left(1 + \frac{n}{R}\right) N(U)\right]$$

$$+ \frac{\partial}{\partial \phi}\left[\left(1 + \frac{n}{R}\right) P(U)\right] + Q(U) = 0 \qquad \text{(C-1)}$$

Differentiating Equation C-1 with respect to s and taking the limit as $r \to 0$, one obtains

$$\frac{\partial}{\partial t}\left[\left(1 + \frac{n}{R_o}\right) U\right] + 2\frac{\partial M}{\partial s} + \frac{\partial}{\partial n}\left[\left(1 + \frac{n}{R_o}\right) N\right] + \frac{\partial}{\partial s}\left[\frac{\partial P}{\partial \phi}\right] + \frac{1}{R_o} N$$

$$+ \frac{1}{\left(1 + \frac{n}{R_o}\right)}\left\{-\frac{n}{R_o^2}\left(\frac{\partial R}{\partial s}\right)_o \left(M + \frac{\partial P}{\partial \phi}\right) + \frac{\partial Q}{\partial s}\right\} = 0 \qquad \text{(C-2)}$$

A conventional application of L'Hospital's rule was not possible in obtaining this limiting form because v_s at the axis does not vanish in the asymmetric case.

Near $s = 0$, $R = R_o$ = constant (hemispherical coordinate system reference surface), therefore, $(\partial R/\partial s)_o = 0$. In addition, at $s = 0$

$$v_s = v_{s_o} \cos\phi$$

$$v_\phi = -v_{s_o} \sin\phi$$

where $v_{s_o}(s, n)$ is the value of v_s in the plane $\phi = 0$ ($v_{s_o} = 0$ for $\alpha = 0$).

For convenience, the calculations are performed in the $\phi = 0$ plane. Dropping the ϕ-momentum equation because $(\partial v_\phi/\partial t)_{s=0} = 0$, Equation C-2 reduces to

$$\frac{\partial}{\partial t}\left[\left(1 + \frac{n}{R_o}\right) U_o\right] + 2\frac{\partial M_o}{\partial s} + \frac{\partial}{\partial n}\left[\left(1 + \frac{n}{R_o}\right) N_o\right] + \frac{\partial}{\partial s}\left[\frac{\partial P_o}{\partial \phi}\right] + Q_o = 0 \qquad \text{(C-3)}$$

where

$$U_o = \begin{bmatrix} \rho \\ \rho v_s \\ \rho v_n \\ \rho E \end{bmatrix}, \quad M_o = \begin{bmatrix} \rho v_s \\ \rho v_s^2 + p \\ \rho v_s v_n \\ \rho v_s (E + p/\rho) \end{bmatrix}, \quad N_o = \begin{bmatrix} \rho v_n \\ \rho v_n v_s \\ \rho v_n^2 + p \\ \rho v_n (E + p/\rho) \end{bmatrix},$$

$$P_o = v_\phi U_o$$

and

$$Q_o = \frac{1}{R_o} \begin{bmatrix} \rho v_n \\ 2\rho v_s v_n - R_o \frac{\partial}{\partial s}(\rho v_\phi^2 + p) \\ \rho(v_n^2 - v_s^2) - p \\ \rho v_n (E + p/\rho) \end{bmatrix}$$

The shock layer transformation (Subsection 2. 2) requires use of the following differential operators:

$$\frac{\partial}{\partial t} = \frac{\partial}{\partial \tilde{t}} + G \frac{\partial F}{\partial t} \frac{\partial}{\partial \tilde{n}} \quad , \quad G = - \frac{n-f}{(F-f)^2}$$

$$\frac{\partial}{\partial s} = \frac{\partial}{\partial \tilde{s}} + H \frac{\partial}{\partial \tilde{n}} \quad , \quad H = - \frac{1}{F-f} \frac{\partial f}{\partial s} + G \left(\frac{\partial F}{\partial s} - \frac{\partial f}{\partial s} \right)$$

$$\frac{\partial}{\partial n} = \frac{1}{F-f} \frac{\partial}{\partial \tilde{n}}$$

$$\frac{\partial}{\partial \phi} = \frac{\partial}{\partial \tilde{\phi}} + G \frac{\partial F}{\partial \phi} \frac{\partial}{\partial \tilde{n}}$$

The additional second-order differential operator required for the axis equations is given by

$$\frac{\partial}{\partial s} \left[\frac{\partial}{\partial \phi} \right] = \frac{\partial}{\partial \tilde{s}} \left[\frac{\partial}{\partial \tilde{\phi}} \right] + \frac{\partial}{\partial \tilde{s}} \left[G \frac{\partial F}{\partial \phi} \frac{\partial}{\partial \tilde{n}} \right] + H \left\{ \frac{\partial}{\partial \tilde{n}} \left[\frac{\partial}{\partial \tilde{\phi}} \right] + \frac{\partial}{\partial \tilde{n}} \left[G \frac{\partial F}{\partial \phi} \frac{\partial}{\partial \tilde{n}} \right] \right\}$$

At s = 0, since

$$\left[\partial F / \partial \phi \right]_o = \left[\partial / \partial \tilde{n} (\partial F / \partial \phi) \right]_o = 0,$$

$$\left\{ \frac{\partial}{\partial s} \left[\frac{\partial}{\partial \phi} \right] \right\}_o = \left\{ \frac{\partial}{\partial \tilde{s}} \left[\frac{\partial}{\partial \tilde{\phi}} \right] + \frac{\partial}{\partial \tilde{s}} \left[\frac{\partial F}{\partial \phi} \right] G \frac{\partial}{\partial \tilde{n}} + H \frac{\partial}{\partial \tilde{n}} \left[\frac{\partial}{\partial \tilde{\phi}} \right] \right\}_o$$

Applying the transformation relations at the axis, Equation C-3 becomes

$$(1 + \frac{n}{R_o}) \left[\frac{\partial U_o}{\partial \tilde{t}} + G_o \left(\frac{\partial F}{\partial t} \right)_o \frac{\partial U_o}{\partial \tilde{n}} \right] + 2 \frac{\partial M_o}{\partial \tilde{s}} + \frac{1}{F_o - f_o} \frac{\partial}{\partial \tilde{n}} \left[(1 + \frac{n}{R_o}) N_o \right]$$

$$+ 2 H_o \frac{\partial M_o}{\partial \tilde{n}} + \left(\frac{\partial v_{s_o}}{\partial \tilde{s}} - H_o \frac{\partial v_{s_o}}{\partial \tilde{n}} \right) U_o - \left(\frac{\partial U_o}{\partial \tilde{s}} + H_o \frac{\partial U_o}{\partial \tilde{n}} \right) v_{s_o} + Q_o = 0 \qquad \text{(C-4)}$$

Evaluation of the finite difference analog of Equation C-4 is performed in upper half of the plane of symmetry ($\phi = 0$).

Appendix D
DETERMINATION OF UPSTREAM FLARE SHOCK CONDITIONS

The nonuniform conditions immediately upstream of the moving flare shock must be determined for each time step during the calculation. A set of logical geometric tests are applied to establish the location of a given flare shock point relative to the converged forebody shock layer network. Flare shock points lying above the bow shock are treated directly using free-stream conditions. The remaining points are located within a given network element, for example, the quadrilateral I-II-III-IV shown in Figure D-1. An interpolation procedure is then applied to determine values of the forebody shock layer properties at the flare shock point in question. The interpolation scheme used in the present analysis is described in detail below.

A set of relations can be derived which transform an arbitrary quadrilateral in the (x, r) plane into a unit square in the (u, v) plane (Figure D-2). Letting

$$x = a_x u + b_x v + c_x uv + d_x$$

$$r = a_r u + b_r v + c_r uv + d_r$$

the coefficients can be evaluated in terms of the coordinates of four arbitrary points in the (x, r) plane which define the quadrilateral in question

$$a_x = x_{10} - x_{00} \qquad d_r = r_{10} - r_{00}$$

$$b_x = x_{01} - x_{00} \qquad b_r = r_{01} - r_{00}$$

$$c_x = x_{11} + x_{00} - (x_{10} + x_{01}) \qquad c_r = r_{11} + r_{00} - (r_{10} + r_{01})$$

$$d_x = x_{00} \qquad d_r = r_{00}$$

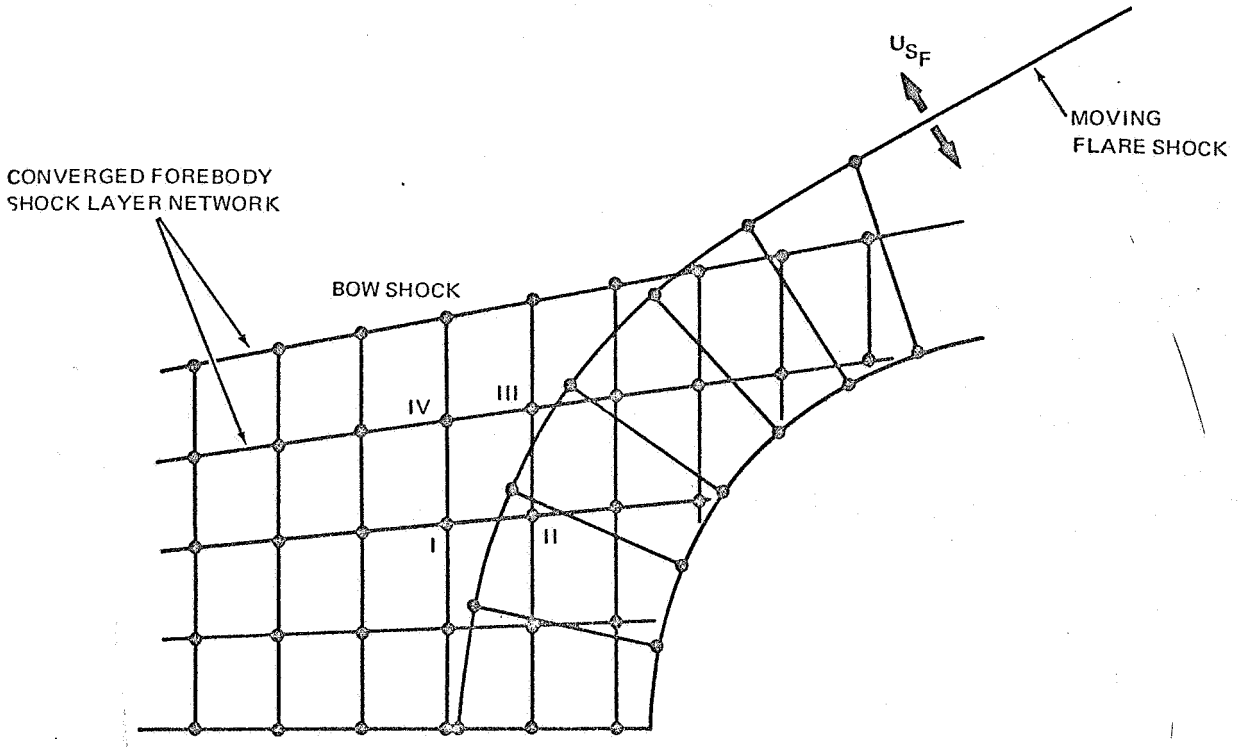

Figure D-1. Representative Forebody and Flare Shock Layer Networks

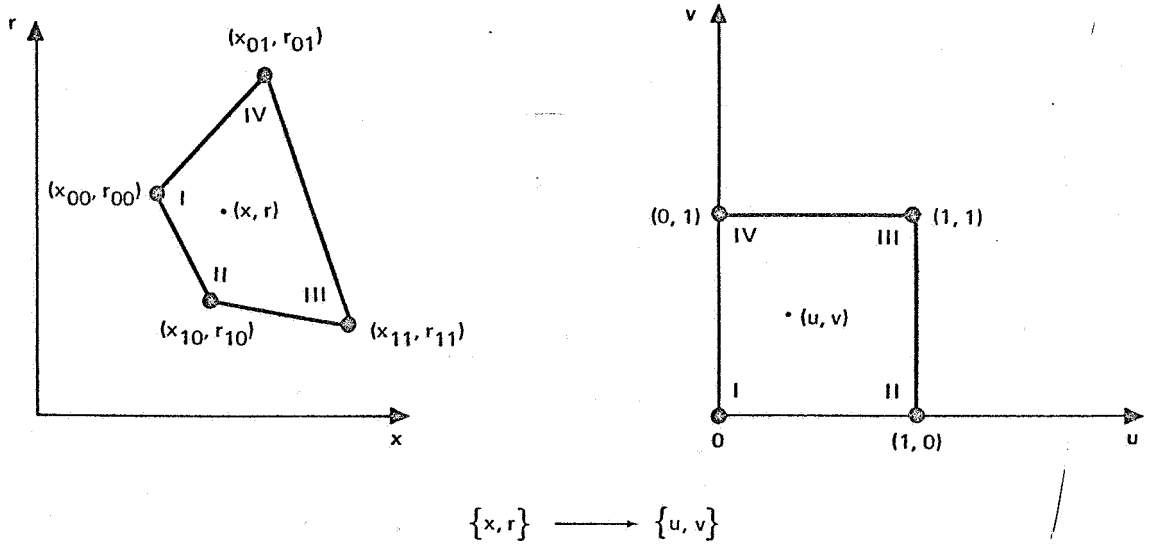

Figure D-2. Geometric Weighting Factor Transformation

Because the points must form a closed figure, they must be identified in cyclic fashion, e.g., points (x_{00}, r_{00}) and (x_{11}, r_{11}) cannot form a side of the quadrilateral.

Solving for u and v in terms of a point (x, r) contained within the quadrilateral

$$u = \frac{r - b_r v - d_r}{a_r + c_r v}$$

where

$$v = \frac{-B \pm [B^2 - 4AC]^{1/2}}{2A} \qquad \text{(sign chosen such that } 0 \leq v \leq 1\text{)}$$

and

$$A = b_x c_r - b_r c_x$$

$$B = r c_x - x c_r + d_r b_x - a_x b_r + c_r d_x - c_x d_r$$

$$C = d_x (r - d_r) - d_r (x - d_x)$$

Using the geometric weighting factors u and v corresponding to a given point (x, r) in the quadrilateral, any flow property, q, can be evaluated at (x, r) using the relation

$$q = au + bv + cuv + d$$

where

$$a = q_{10} - q_{00}$$

$$b = q_{01} - q_{00}$$

$$c = q_{11} + q_{00} - (q_{10} + q_{01})$$

$$d = q_{00}$$

and $q_{ij} = q(x_{ij}, r_{ij})$